DMD Fast Forward. Published on October 2, 2012 as doi:10.1124/dmd.112.048264
This article has not been copyedited and formatted. The final version may differ from this version.

DMD #048264

Discovery and Characterization of Novel, Potent, and Selective Cytochrome P450 2J2 Inhibitors

Shuang Ren, Juan Zeng, Ye Mei, John Z. H. Zhang, S. Frank Yan, Jian Fei, and Li Chen

School of Life Science and Technology, Tongji University, Shanghai 200092, China (SR, JF, LC); Non-Clinical Safety, Roche Pharma Research and Early Development China, Shanghai 201203, China (SR); Medicinal Chemistry, Roche Pharma Research and Early Development China, Shanghai 201203, China (JZ, SFY); State Key Laboratory of Precision Spectroscopy, Department of Physics, Institute of Theoretical and Computational Science, East China Normal University, Shanghai 200062, China (JZ, YM, JZHZ); Department of Chemistry, New York University, New York, New York 10003, USA (JZHZ)

Running title: Discovery of novel, potent, and selective CYP2J2 inhibitors

Corresponding author address:

Li Chen, Ph.D.

School of Life Science and Technology, Tongji University

1239 Si Ping Road

Shanghai 200092

lichen@huamedicine.com

Number of text pages: 41

Number of tables: 4

Number of figures: 8

Number of References: 59

Words in Abstract: 249

Words in Introduction: 749

Words in Discussion: 1500

List of abbreviations: astemizole (AST), cytochrome P450 (CYP), cytochrome P450 2J2 (CYP2J2), drug-drug interaction (DDI), *O*-desmethyl astemizole (DES-AST), human liver microsome (HLM), liquid chromatography-tandem mass spectrometry (LC-MS/MS), nicotinamide adenine dinucleotide phosphate (NADPH), time-dependent inhibition (TDI)

Abstract

Cytochrome P450 (CYP) 2J2 is one of the human CYPs involved in phase I xenobiotics metabolism. It is mainly expressed in extrahepatic tissues including intestine and cardiovascular systems. The general role of CYP2J2 in drug metabolism is not yet fully understood, while the recent discovery that CYP2J2 can metabolize a wide range of structurally diverse drugs and its primary distribution in the intestine suggest its potentially indispensable role in first-pass intestinal metabolism and involvement in drug-drug interaction (DDI). To fully characterize its role in drug metabolism selective and potent inhibitors of CYP2J2 are necessary tools. In the current study, 69 known drugs have been screened for the inhibition of CYP2J2 and we have discovered a number of marketed drugs as potent and selective CYP2J2 inhibitors. In particular, telmisartan and flunarizine have CYP2J2 inhibition IC50 values of 0.42 and 0.94 μM, respectively, which are at least 10-fold more selective against all other major metabolizing CYPs; moreover, they are not substrate of CYP2J2 and show no time-dependent inhibition (TDI) toward this CYP. The results of enzyme kinetics studies, supported by molecular modeling, have also elucidated that telmisartan is a mixed type inhibitor while flunarizine competitively inhibits CYP2J2. The K_i for telmisartan is 0.19 μM with an α value, an indicator of the type of inhibition mechanism, of 2.80, while flunarizine has a K_i value of 0.13 μM. These newly discovered CYP2J2 inhibitors can be potentially used as a tool to study CYP2J2 in drug metabolism and interaction in a clinical setting.

Introduction

Cytochrome P450 (CYP) 2J2 is one of the human CYPs involved in metabolic transformation of xenobiotics. It is mainly expressed in intestine and cardiovascular systems including endothelium and myocardiocytes with however low expression level in the liver (Node et al., 1996; Wu et al., 1996; Delozier et al., 2007; Xu et al., 2011). Endogenously, CYP2J2 is the epoxygenase that oxidizes arachidonic acid (AA) to regioisomeric *cis*-epoxyeicosatrienoic acids (EETs), an important class of bioactive eicosanoids (Oliw, 1994; Capdevila et al., 2000; Brash, 2010; Guengerich and Rendic, 2010) that exhibits a wide range of cardiovascular protective effects (Baron et al., 1997; Imig et al., 1999; Fleming, 2004; Seubert et al., 2004; Larsen et al., 2006; Xiao et al., 2010). In recent years CYP2J2 and its EET metabolites have also been implicated in the pathological development of human cancers for both solid tumors and hematological malignancies (Jiang et al., 2005; Freedman et al., 2007; Jiang et al., 2007; Chen et al., 2009; Chen et al., 2011).

On the other hand, the role that CYP2J2 plays in drug metabolism is not yet fully understood. Previous studies have identified a number of drugs from different disease areas that can be metabolized by CYP2J2, including astemizole, ebastine, terfenadine and vorapaxar (Matsumoto and Yamazoe, 2001; Matsumoto et al., 2002; Liu et al., 2006; Lee et al., 2012). More importantly, it is indicated that CYP2J2 plays a dominant role in the first-pass intestinal metabolism of ebastine to its pharmacologically active metabolite carebastine (Hashizume et al., 2002; Matsumoto et al., 2002; Lee et al., 2010). In a recent publication a number of structurally diverse substrates of CYP2J2 have been identified ranging from albendazole with a molecular weight of only 265 to complex molecules such as cyclosporine with a molecular weight of 1201 (Lee et al., 2012). With

its rather broad substrate spectrum and unique tissue distribution pattern, it is possible that CYP2J2 can influence drug metabolism in the extrahepatic tissues, particularly the intestine, which may therefore dominate first-pass metabolism for certain drugs and cause drug-drug interaction (DDI) in the gastrointestinal tract. Indeed, the latest guidance for industry on drug interaction studies from the U.S. Food and Drug Administration (FDA) suggests that CYP2J2 should be considered if a new drug candidate is found to be not metabolized by the major CYPs, indicating the increasingly more recognized role of CYP2J2 in drug metabolism (US Department of Health and Human Services, 2012).

In order to fully characterize CYP2J2 in drug metabolism both in vitro and in vivo, the specific metabolic reactions mediated by CYP2J2 and the potent and selective inhibitors against this CYP isoform are indispensible tools. Using recombinant CYP2J2 enzyme, screening of substrate and inhibitor of this CYP isoform can be performed, as specific substrate can be useful for profiling CYP2J2 inhibition of drug candidates in vitro in liver microsome using cocktail method while specific potent CYP2J2 inhibitor can also facilitate the evaluation of the role that CYP2J2 plays in liver microsomal metabolism and DDI in vivo. Several metabolic reactions have been reported to date to be primarily mediated by CYP2J2, which include astemizole *O*-demethylation, ebastine hydroxylation, and recently identified amiodarone 4-hydroxylation (Matsumoto et al., 2002; Liu et al., 2006; Lee et al., 2012). These specific reactions can be useful tools to determine CYP2J2 activity and its roles in drug metabolism. Moreover, the specific tool inhibitor preferably shall not be the substrate of CYP2J2, as it would otherwise add unnecessary complexity in both experimental design and data analysis. Unfortunately, only very few marketed drugs are found to be non-CYP2J2 substrate, but exhibiting potent and selective CYP2J2 inhibition. In one study, Lafite et al. reported a tool

compound derived from terfenadine as potent CYP2J2 inhibitor without knowing however its selectivity against several major CYPs including CYP2D6 and CYP1A2 (Lafite et al., 2007). Very recently Lee et al. screened a library of 138 marketed drugs and showed 42 of them had CYP2J2 inhibitory activity greater than 50% at a single compound concentration of 30 μM (Lee et al., 2012). Among them danazol was shown to be a potent CYP2J2 inhibitor with a K_i value of 20 nM, albeit that it also inhibits other key CYPs such as CYP2C9 and CYP2D6 with IC50 values at single digit μM range. It is noted that all of them are CYP2J2 substrates and mechanistically characterized as competitive CYP2J2 inhibitor (Lafite et al., 2007; Lee et al., 2012). Given the increasingly important role CYP2J2 plays in drug metabolism and first-pass intestinal metabolism in particular, it is essential to expand our repertoire of tool drugs with potent and selective CYP2J2 inhibition, preferably a non-substrate compound, to facilitate the study for CYP2J2-mediated drug metabolism and clinically relevant drug-drug interaction potential.

In the current study, we selected 69 known drugs and tested their inhibitory activity against astemizole *O*-demethylation, a well-known reaction catalyzed by CYP2J2. Among them, 12 compounds were showed to have an IC50 value less than 10 μM. Specifically, telmisartan, flunarizine, norfloxacin and metoprolol were found to be selective inhibitors against CYP2J2 in the sub-μM range. Both telmisartan and flunarizine were also demonstrated to be the non-substrate inhibitors of CYP2J2. Telmisartan also exhibits a mixed type inhibition mechanism while flunarizine shows a competitive inhibition, consistent with the computer modeling studies at a molecular and thermodynamic level. In conclusion, a number of currently marketed drugs have been discovered as CYP2J2 inhibitors that can be potentially used as new tools to study the

role of CYP2J2 in drug metabolism and its potential involvement in drug-drug interaction in a clinical setting.

Materials and Methods

Materials. CYP substrates, inhibitors, metabolite standards, and all other materials were obtained from the following sources: all compounds from Table 1, except olmesartan, that were used as inhibitors for the CYP2J2 and human liver microsome (HLM) inhibition studies, astemizole (AST), phenacetin, tolbutamide, bufuralol, omeprazole, 4'-hydroxytolbutamide, 1'-hydroxybufuralol, 6β-hydroxytestosterone, acetaminophen, dextrorphan, and nicotinamide adenine dinucleotide phosphate (NADPH) were purchased from Sigma-Aldrich (St. Louis, MO, USA); testosterone was purchased from Acros Organics (Morris Plains, NJ, USA); 5'-hydroxyomeprazole was purchased from Toronto Research Chemicals Inc. (North York, ON, Canada); olmesartan and *O*-desmethyl astemizole (DES-AST) were purchased from Santa Cruz Biotechnology (Santa Cruz, CA, USA); potassium phosphate (monobasic and dibasic) and magnesium chloride hexahydrate ($MgCl_2$) were purchased from Merck (Darmstadt, Germany); pooled HLMs and recombinant CYP enzyme were purchased from BD Gentest (Woburn, MA, USA); high-performance liquid chromatography (HPLC) grade dimethyl sulfoxide (DMSO), methanol, and formic acid used for liquid chromatography-tandem mass spectrometry (LC-MS/MS) analysis were purchased from Fisher Scientific Co. (Pittsburgh, PA, USA).

CYP2J2 Activity Study. Astemizole *O*-demethylation, a well-known reaction catalyzed by CYP2J2, was measured and characterized in all studies to evaluate CYP2J2 activity, and hereafter it will be the functional assay used for CYP2J2 activity. The substrate, astemizole, was diluted sequentially by DMSO to yield the final required

DMD Fast Forward. Published on October 2, 2012 as DOI: 10.1124/dmd.112.048264
This article has not been copyedited and formatted. The final version may differ from this version.

concentration. The reaction mixtures contained a final concentration of 0.05 M sodium potassium phosphate buffer (pH=7.4), 5 pmol/mL CYP2J2, 1 mM NADPH, and substrate concentrations ranging from 0.1 to 20 μM, in a total volume of 200 μL. The DMSO concentration was 0.25% v/v. The reaction was initiated by the addition of NADPH after 5 minutes of pre-incubation at 37°C and was terminated 10 minutes after incubation by adding 150 μL of ice cold methanol containing 100 ng/mL of tolbutamide (internal standard) into 50 μL of the reaction mixtures. The standard solution of DES-AST was prepared and treated in the exact same way as the parent compound except without having the NADPH to yield final concentrations from 0.2 to 10 nM. After being vortexed for 1 minute and centrifuged at 4000 RPM under 4°C for 10 minutes, the clear supernatant was then used directly for LC-MS/MS analysis.

CYP2J2 Inhibition Study. Compounds used in the CYP2J2 inhibition study were dissolved and diluted sequentially in DMSO to ensure that the final DMSO concentration was 0.1% v/v in each sample. All samples were incubated in duplicate. The incubation mixture consisted of 0.1 M sodium potassium phosphate buffer (pH=7.4), 1 pmol/mL recombinant CYP, 0.15 μM AST, and 0.5 mM NADPH in a final volume of 200 μL, with various inhibitor concentration of 0.023 to 50 μM. The reaction was initiated by addition of NADPH after 10 minutes of pre-warming at 37°C and was terminated 10 minutes after incubation by adding 100 μL of ice cold methanol containing 100 ng/mL of tolbutamide (internal standard) into the mixtures. After being vortexed for 1 minute and centrifuged at 4000 RPM under 4°C for 10 minutes, the clear supernatant was used directly for LC-MS/MS analysis.

Human Liver Microsome Inhibition Study. Compound selectivity was assessed by its inhibitory potential against five major CYPs, namely CYP3A4, CYP2D6,

DMD Fast Forward. Published on October 2, 2012 as DOI: 10.1124/dmd.112.048264
This article has not been copyedited and formatted. The final version may differ from this version.

CYP2C9, CYP2C19, and CYP1A2. A cocktail method that enables simultaneous incubation and measurement of compound inhibitory activity against each CYP isoform was developed with modification from previously reported (Testino and Patonay, 2003; Weaver et al., 2003; Walsky and Obach, 2004). Each incubated mixture contained 0.125 mg/mL HLM (protein content), 5 mM $MgCl_2$, 100 mM potassium phosphate buffer (pH= 7.4), substrate cocktail, various concentrations of test compound and 2 mM NADPH in a total volume of 200 μL. The final DMSO concentration was 0.25% v/v. The final concentrations of each CYP substrate were at the reported literature K_m values (Testino and Patonay, 2003; Weaver et al., 2003; Walsky and Obach, 2004), respectively (Table 2). Before addition of NADPH to initiate the reaction, mixtures were pre-warmed at 37°C for 10 minutes. Reaction was terminated after 15 minutes by adding 100 μL of ice cold methanol containing 3 μM dextrorphan as an internal standard. Samples were then centrifuged at 4000 RPM for 10 minutes at 4°C. The supernatant was then analyzed by LC-MS/MS.

Telmisartan and Flunarizine CYP2J2 Metabolic Stability. In order to evaluate whether telmisartan and flunarizine are the substrate of CYP2J2, the CYP2J2 metabolic stability of the two compounds were measured. Astemizole was used as positive control. Each incubated mixture contained 70 pmol/mL human recombinant CYP2J2, 100 mM potassium phosphate buffer (pH=7.4), 1 mM NADPH, and 1 μM of test compound in a total volume of 400 μL. After pre-warm at 37°C for 10 minutes, the NADPH was added to initiate the reaction. Reaction was terminated after 0, 3, 6, 9, 15, and 30 minutes by adding 150 μL of 100 ng/mL of tolbutamide (internal standard) in ice cold methanol into 300 μL of incubation mixtures. The incubation was performed in duplicate. Samples were then centrifuged at 4000 RPM for 10 minutes at 4°C. The

DMD Fast Forward. Published on October 2, 2012 as DOI: 10.1124/dmd.112.048264
This article has not been copyedited and formatted. The final version may differ from this version.

supernatant was then analyzed by LC-MS/MS. The metabolic stability of telmisartan and flunarizine in HLM was also evaluated by incubating the compound (1 μM) in a mixture containing 0.5 mg/mL human liver microsome, 100 mM potassium phosphate buffer (pH=7.4), and 10 mM NADPH for 30 minutes. The quenching procedure was the same as in the **CYP2J2 Inhibition Study** section. Samples were then centrifuged at 4000 RPM for 10 minutes at 4°C and supernatant was analyzed by LC-MS/MS.

Time-dependent Inhibition Study. The time-dependent inhibition (TDI) of CYP2J2 by telmisartan and flunarizine was measured based on a traditional IC50 shift method. Test compounds were pre-incubated at eight different concentrations (from 0.023 to 50 μM) with recombinant CYP2J2 protein (1 pmol/mL) in the presence and absence of NADPH (1 mM) for 30 minutes. The reaction was initiated by adding 0.15 μM astemizole and incubated for 10 minutes. The quenching procedure was the same as in the **CYP2J2 Inhibition Study** section. Samples were then centrifuged at 4000 RPM for 10 minutes at 4°C and supernatant was analyzed by LC-MS/MS.

Analytical Method. All samples were analyzed on an Applied Biosystems API 4000 triple quadrupole mass spectrometer coupled with an Agilent 1200 HPLC system. For AST and DES-AST detection, the chromatographic separation was carried out on a Phenomenex Synergy Hydro-RP column (50×3.0 mm, 4 μm particles) with the gradient of 30%-100%-100%-30%-30% B was applied at 0-0.3-1.8-1.9-3.0 minute marks, respectively, in which the mobile phases A and B were water and methanol (both containing 0.1% formic acid), respectively, at a flow rate of 0.6 mL/min an injection volume of 5 μL. The mass spectrometer was operated under the positive ion detection mode using the transitions m/z 459→218 for AST, m/z 445→204 for DES-AST, and m/z 271→172 for tolbutamide, respectively. The collision energy was 35, 30, and 18 eV for

AST, DES-AST, and IS, respectively. The calibration curves were fitted by the least-square regression of the peak area ratio of DES-AST to tolbutamide (y) versus DES-AST concentration (x), using $1/x^2$ as the weighting factor. For telmisartan and flunarizine metabolic stability test, the same HPLC method was used. The mass reactions used for measuring telmisartan and flunarizine were m/z 515→276 and m/z 405→203, respectively, under the positive ion detection mode. The collision energy was 52 and 14 eV for telmisartan and flunarizine, respectively. For samples from the HLM inhibition studies, similar analytical method was applied with the adjusted gradient elution program as followed: 10%-10%-40%-65% B was applied at 0-0.5-0.8-1.1 minute marks, respectively, followed by 2.4 minutes isocratic elution with 65% B and column equilibration, resulting in a total time of 5 minutes per injection. The multiple reaction monitoring (MRM) parameters of the LC-MS/MS for each metabolite and IS were summarized in Table 2.

Enzyme Kinetics Study. The mechanism of inhibition of telmisartan and flunarizine was characterized by enzyme kinetics. The substrate (AST) at various concentrations ranging from 0.05 to 0.45 μM was co-incubated with the inhibitor in a concentration range of 0.2 to 2 μM for telmisartan and 0.2 to 5 μM for flunarizine, respectively, in order to determine their K_i values (n = 4). The reaction conditions, sample preparation, standard curve preparation, and sample analysis were the same as described above in the **CYP2J2 Activity Study** and **Analytical Method** sections.

Data Analysis and Statistics. The XL*fit* 4.2.1 software (ID Business Solutions Ltd., Guildford,UK) was used to compute the enzyme kinetics parameters including K_m, V_{max}, and IC50. The models 253 (Michaelis–Menten steady state model) and 205 (four-

parameter logistic model) were used for activity and inhibition calculations, respectively. A combination of both graphical and statistical approaches was used to determine the most suitable inhibition model, i.e., competitive, non-competitive, mixed, or uncompetitive. Specifically, the Dixon plots were used as the graphical method and more importantly the non-linear regression analysis played a dominant role in determining the type of inhibition. The statistical parameters from the non-linear regression analysis were obtained using GraphPad Prism 5.01 (GraphPad Software, Inc., La Jolla, CA, USA), which include R^2 value, standard deviation of the residuals (Sy.x), and a sum-of-squares *F*-test. Specifically, for simple models, it was determined by the best R^2 and the smallest Sy.x values, while for complex model, the *F*-test was used to test whether or not a complex model (with added parameters) would be a better fit. When a *p*-value smaller than 0.05 is observed, the complex model is accepted, otherwise the simple model will be accepted. The estimated K_i was then determined based on the selected inhibition model. The following equations were used to determine the K_i value for each model, respectively:

Competitive:

$$v = V_{max} \times [S]/([K_m \times (1 + [I]/K_i)] + [S])$$

Non-competitive:

$$v = V_{max} \times [S]/[K_m \times (1 + [I]/K_i) + [S] \times (1+ [I]/K_i)]$$

Linear mixed:

$$v = V_{max} \times [S]/[K_m \times (1+ [I]/K_i) + [S] \times (1 + [I]/ \alpha K_i)]$$

Uncompetitive:

$$v = V_{max} \times [S]/[K_m + [S] \times (1+ [I]/K_i)]$$

DMD Fast Forward. Published on October 2, 2012 as DOI: 10.1124/dmd.112.048264
This article has not been copyedited and formatted. The final version may differ from this version.

where *v* is the reaction rate, V_{max} (pmol/min/nmol protein) is the maximum reaction rate, K_m (μM) is the Michaelis–Menten constant, K_i (μM) is the inhibitor constant, [I] (μM) is the inhibitor concentration, [S] (μM) is the substrate concentration, and α is a factor by which the K_i changes in the presence of substrate.

Molecular Modeling and Dynamics Simulation. A previously published CYP2J2 homology model (Li et al., 2008) was used for the docking study. The protein was prepared by the Protein Preparation Wizard module in the Schrödinger suite of programs and the ligands were prepared by the LigPrep module. All docking studies were carried out using the Glide module (Friesner et al., 2004; Halgren et al., 2004) and both the Glide docking score and visual inspection were applied to select the most suitable poses for subsequent dynamics simulation.

Regarding the initial structure, the entire system contains three parts: the protein, heme, and ligand. The parameters for the protein were from the force field 99SB (FF99SB) in the AMBER11 package (Case et al., 2005). D. Giammnona provided the heme parameter (Giammona, 1984) in the AMBER11 package. As for the ligand, we used the following standard procedure to prepare the parameters. First, we minimized the ligands with Gaussian 09 at the HF/6-31G* level (Frisch et al., 2009). The minimized structure was then used to calculate the single-point electrostatic potential at HG/6-31G* level. Using the resultant electrostatic potential, we applied the RESP (Bayly et al., 1993) model in AMBER11 to fit the partial charges of the ligand. The generalized AMBER force field (GAFF) parameters (Wang et al., 2004) were then applied for the ligand. The whole system was solvated in a periodic box of TIP3P waters (Jorgensen et al., 1983), and the minimum distance from the surface atom to the edge of the box was set to 12 Å. Counterions were also added to neutralize the entire system.

DMD Fast Forward. Published on October 2, 2012 as DOI: 10.1124/dmd.112.048264
This article has not been copyedited and formatted. The final version may differ from this version.

The molecular dynamics (MD) simulations were carried out using the AMBER11 package. The cutoff for the long range interaction was set at 10 Å and the particle mesh Ewald (PME) method (Darden et al., 1993) was applied to treat the long range electrostatic interaction. The SHAKE algorithm (Miyamoto and Kollman, 1992) was applied to restrain all bonds involving the hydrogen atoms. The simulations followed the same protocol. First, all the water molecules, counterions, and hydrogen atoms were minimized for 20000 steps by the steepest descent approach followed by 30000 steps of conjugate gradient minimization with rest the system fixed. The whole system was further minimized using conjugate gradient to convergence with a criteria of 10^{-4} kcal/mol/Å of the root-mean-square of the Cartesian elements of the gradient. The system was then gradually heated from 0 to 300 K for 100 ps with a 10.0 kcal/mol/$Å^2$ restraining force applied on the protein-ligand complex. The Langevin dynamics temperature coupling scheme was applied (Pastor et al., 1998) and the collision frequency was set at 2.0 ps^{-1}. Finally, we completely relaxed the whole system and ran the production simulation for 2 ns using the NPT ensemble with a time step of 2 fs.

Binding Free Energy Calculation. A total of 100 snapshots were extracted at 2 ps interval from the last 200 ps simulation for the binding free energy calculation. The protein together with the heme was defined as the receptor. The molecular mechanics generalized Born surface area (MM-GBSA) method (Qiu et al., 1997) was applied to compute the binding free energy between the ligand and the receptor. The total binding energy can be expressed as:

$$\Delta G_{bind} = G_{complex} - G_{receptor} - G_{ligand}$$

$$= \Delta H - T\Delta S$$

$$= \Delta E_{elec} + \Delta E_{vdW} + \Delta G_{GB} + \Delta G_{nonpolar} - T\Delta S$$

where ΔE_{elec} is the electrostatic contribution to the binding free energy and ΔE_{vdW} is the van der Waals interaction contribution. Both electrostatic and van der Waals interaction energies were calculated using the SANDER module from the AMBER11 package. We applied the modified generalized Born (GB) model developed by Onufriev and colleagues (Onufriev et al., 2000) (referred as GB^{OBC}) to calculate the electrostatic and van der Waals interaction energies without any cutoff. ΔG_{GB} and $\Delta G_{nonpolar}$ represent the electrostatic and nonpolar contributions to the solvation free energy, respectively. The GB method in AMBER11 was used to compute the electrostatic part, $\Delta G_{GB,}$ where the exterior dielectric constant was 80 and the interior dielectric constant was 1. The ionic strength for the GB solvent is 0, so the electrostatic screening effects of salt is not considered here. The Bondi radii (Bondi, 1964) were used for all atoms. It is noteworthy that we set the F atom radius to 1.47 Å (Batsanov, 2001), which is not included in the standard AMBER11 package. The nonpolar contribution ($\Delta G_{nonpolar}$) is calculated using the LCPO method (Weiser et al., 1999) and can be expressed as:

$$\Delta G_{nonpolar} = SURFTEN \times SASA + SURFOFF$$

The SASA is the solvent-accessible surface area obtained from the MOLSURF program (Connolly, 1983) and the SURFTEN and SURFOFF parameters were 0.0072 and 0, respectively. The radius of probe sphere was set 1.4 Å. The entropic contribution ($T\Delta S$) to the binding free energy was not considered in our calculation.

Results

DMD Fast Forward. Published on October 2, 2012 as DOI: 10.1124/dmd.112.048264
This article has not been copyedited and formatted. The final version may differ from this version.

CYP2J2 Enzymatic Activity Was Determined by Astemizole *O*-demethylation Reaction. The astemizole *O*-demethylation reaction was used to characterize the metabolic/enzymatic activity of CYP2J2 as this biotransformation is well known to be catalyzed primarily by CYP2J2 in human (Matsumoto et al., 2002; Lee et al., 2012). The metabolizing activity of CYP2J2 for astemizole *O*-demethylation was measured to ensure that substrate concentration used in the follow-up inhibition studies was suitably around the K_m value. Under our experimental conditions, the apparent kinetic parameters of astemizole *O*-demethylation using recombinant human CYP2J2 were determined as the followings: K_m = 0.09 ± 0.01 μM and V_{max} = 339 ± 13.0 pmol/min/nmol protein (n = 2).

Telmisartan and Flunarizine Show Significant and Selective Inhibition against CYP2J2. A total of 69 marketed drugs were screened by using this in vitro astemizole *O*-demethylation system to characterize their inhibitory effect on CYP2J2 activity. The results are shown in Table 3. Out of the 69 compounds, 20 of them inhibit the CYP2J2 metabolizing activity with an IC50 value less than 50 μM, while 12 compounds even show IC50 values < 10 μM. Three most potent compounds, namely telmisartan, flunarizine, and amodiaquine, exhibit sub-μM potency against CYP2J2 with IC50 values of 0.42, 0.94, and 0.99 μM, respectively. The concentration-dependent inhibition curves for telmisartan and flunarizine are shown in Figure 1.

In order to evaluate the selectivity of CYP2J2 inhibition and given its predominant expression in the extrahepatic tissues such as intestine, we examined the inhibitory effect of these 20 compounds against five major human CYP isoforms including CYP3A4, CYP2C9, CYP2C19, and CYP2D6 which are also the most abundantly expressed CYP isoforms in the human intestine (Ding and Kaminsky, 2003;

DMD Fast Forward. Published on October 2, 2012 as DOI: 10.1124/dmd.112.048264
This article has not been copyedited and formatted. The final version may differ from this version.

Paine et al., 2006) and CYP1A2. As shown in Table 3, besides inhibition of CYP2J2 telmisartan also inhibits CYP2C9 (IC50 = 4.8 μM), nearly 10-fold less potent comparing to that of CYP2J2. On the other hand, telmisartan does not exhibit any inhibition against other four major CYPs including CYP3A4 and CYP2D6. Similarly, flunarizine only inhibits CYP2D6 with an IC50 of 7.8 μM, which is also about 10-fold less potent than that of CYP2J2, and shows minimum inhibition for other four key CYPs (IC50 > 50 μM). Moreover, amodiaquine is a potent inhibitor for both CYP2J2 (IC50 = 0.99 μM) and CYP2D6 (IC50 = 0.64 μM). In addition, it is noteworthy that both norfloxacin and metoprolol display excellent selectivity for CYP2J2 with IC50 values of 2.6 and 4.9 μM, respectively and are not active against all five major CYPs (IC50s > 50 μM; Table 3).

Telmisartan and Flunarizine Are Non-substrate CYP2J2 Inhibitors. Many CYP inhibitors are also substrates of the isoform they inhibit, especially for those competitive inhibitors that exert their inhibitory power by competing for the same catalytic binding site of the substrate. In this study the metabolic activity of CYP2J2 towards telmisartan and flunarizine was evaluated. The metabolic clearance of astemizole by CYP2J2 was also measured to define the enzyme activity. After incubating for 30 minutes, astemizole was metabolized by CYP2J2 with an intrinsic clearance (CL_{int}) of 3.05 ± 0.07 μL/min/pmol protein (n = 2; Figure 2, panel A). This correlates well with the intrinsic clearance calculated from V_{max} and K_m ($CL_{int} = V_{max}/K_m$ = 3.77 ± 0.05 μL/min/pmol protein), indicating excellent consistency of the CYP2J2 activity between these two studies based on percentage remaining of the substrate astemizole and enzyme kinetics. Importantly, the amount of telmisartan and flunarizine remains almost unchanged after incubation for 30 minutes (CL_{int} = 0.0 μL/min/pmol protein, n = 2; Figure 2, panels B and C). This result clearly shows that both telmisartan

and flunarizine are not substrate of CYP2J2. It is also noted that after incubation of telmisartan and flunarizine in HLM for 30 minutes, the percentage remaining of telmisartan and flunarizine was 97.7% and 83.8%, respectively.

Telmisartan and Flunarizine Show No Time-dependent Inhibition toward CYP2J2. The time-dependent inhibition toward CYP2J2 of the most potent inhibitors, telmisartan and flunarizine, was also investigated. After pre-incubation of the inhibitor with CYP2J2 protein for 30 minutes in the presence and absence of NADPH, the IC50 values of CYP2J2 inhibition were then measured in both cases. The IC50 shift was calculated as IC50 in the absence of NADPH over IC50 in the presence of NADPH. As shown in Figure 3, telmisartan and flunarizine displayed marginal IC50 shift of 1.0 and 1.3, respectively, both of which are smaller than the TDI IC50 shift threshold of 1.5 (Berry and Zhao, 2008), indicating none of them are time-dependent inhibitor of CYP2J2.

Telmisartan and Flunarizine Exhibit Distinctive CYP2J2 Inhibition Kinetics. Detailed inhibition kinetics studies were carried out for both telmisartan and flunarizine and the results are shown in Figure 4. The non-linear regression curves of velocity versus substrate concentration and the Dixon plots of the reciprocal of velocity ($1/v$) versus inhibitor concentration were drawn for the substrate astemizole at 0.05, 0.1, 0.15, 0.3, and 0.45 μM, for telmisartan at 0, 0.2, 0.5, and 2 μM, and for flunarizine at 0, 0.2, 1, and 5 μM, respectively. Visual inspection of the Dixon plots (Figure 4, panels C and D and insets) suggests that both telmisartan and flunarizine could be a competitive or mixed type inhibitor for CYP2J2 with a similar K_i value of about 0.1 μM. Furthermore, as shown in the slope of Dixon plot versus reciprocal of substrate concentration (1/[S]) plots (Figure 4, panels E and F), telmisartan is indicated to be a mixed type inhibitor (i.e., the

plot does not go through the origin) while flunarizine is a competitive inhibitor (i.e., the plot goes through the origin). We then applied the non-linear regression analysis to further confirm the inhibition type of both drugs. When simple models were used, flunarizine inhibition kinetics was best fitted to a competitive model. Subsequently, when we tried to use a more complex mixed model to fit the data, we obtained a *p*-value of 0.78, much greater than the threshold 0.05, indicating that flunarizine is indeed a competitive inhibitor of CYP2J2 with a K_i value of 0.13 ± 0.02 μM. The data of telmisartan inhibition kinetics could be fitted by a non-competitive model. However, those data could be even better fitted by a more complex mixed model, and the *p*-value was 0.039. Based on these model fitting results it was suggested that the inhibition mechanism of telmisartan could be described by a linear mixed type inhibition model. The corresponding K_i of telmisartan is 0.19 ± 0.05 μM with an α value of 2.80 ± 1.39. In overall, these data indicate that flunarizine likely inhibits CYP2J2 enzymatic activity by directly competing with the substrate (in this case astemizole), whereas telmisartan might inhibit the enzyme in an allosteric fashion.

Computer Modeling Studies of the CYP2J2 Inhibition Mechanism by Telmisartan and Flunarizine. In order to further delineate the distinctive inhibition mechanisms of telmisartan and flunarizine as indicated by the inhibition kinetics studies, we set out to apply computational modeling approaches to study the interactions between the inhibitor and CYP2J2 on a molecular level. The CYP2J2 model was previously described by Li and colleagues (Li et al., 2008) and was used as the starting structure in the study. The docking models of the telmisartan–CYP2J2 and flunarizine–CYP2J2 complexes are shown in Figure 5, panels A and B, respectively. Interestingly, telmisartan and flunarizine seem to occupy different regions of the CYP2J2 ligand binding pocket.

DMD Fast Forward. Published on October 2, 2012 as DOI: 10.1124/dmd.112.048264
This article has not been copyedited and formatted. The final version may differ from this version.

We further subjected the two complex systems to all-atom molecular dynamics simulation. The CYP2J2 protein displays limited overall conformational change in both systems, while the inhibitor telmisartan exhibits greater conformational flexibility than flunarizine within the CYP2J2 binding pockets (Figure 5, panels C and D).

As shown in Figure 6, telmisartan binds to a pocket that is remote to the catalytically important heme with a minimum distance between telmisartan and heme of about 8 Å. The pocket is largely comprised of residues of hydrophobic nature, mainly from N-terminal loop and helix A, sheet β1 and associated loops, helix K', sheet β4 and associate loop, K/β1-4 segment, B/C segment, helix F, as well as F/G segment (Figure 6, panels A and C). On the other hand, flunarizine binds directly within the active site of CYP2J2 with the F atom right on top of the heme Fe ion, presumably blocking substrate binding. The binding pocket is also formed primarily by hydrophobic residues, largely from N-terminal loop and helix A, sheet β4 and associate loop, K/β1-4 segment, B/C segment, helix F, as well as helix I and the heme porphyrin ring (Figure 6, panels B and D).

To further study how telmisartan and flunarizine interact with CYP2J2 from a thermodynamics point of view, we carried out MM-GBSA calculation to estimate the inhibitor binding free energy to CYP2J2 (Table 4). The binding free energy (without considering the entropy) between telmisartan and CYP2J2 protein is –55.5 kcal/mol, slightly lower than that for flunarizine (–52.8 kcal/mol). This is consistent with the similar inhibition IC50 values of the two drugs, where telmisartan (0.42 μM) is marginally more potent than flunarizine (0.94 μM). The binding energies observed here are generally in line with structural observation. Specifically, given the predominantly lipophilic nature of the CYP2J2 binding pocket and a larger estimated hydrophobic

DMD Fast Forward. Published on October 2, 2012 as DOI: 10.1124/dmd.112.048264
This article has not been copyedited and formatted. The final version may differ from this version.

surface for telmisartan (432.86 $Å^2$) than in the case of flunarizine (380.83 $Å^2$), it is conceivable that the van der Waals interaction contributes more significantly to the binding of telmisartan than that of flunarizine (Table 4). Moreover, although both telmisartan and flunarizine make one hydrogen bond to the protein, namely Arg484 side chain and Ile487 backbone, respectively, the polar and/or electrostatic interaction between both ligands and the protein is minimum. This is reflected in the unfavorable electrostatic binding free energy in both cases (Table 4), where telmisartan likely has to pay more desolvation penalty than flunarizine, in line with a larger polar surface area in the case of telmisartan (56.19 $Å^2$) than that of flunarizine (8.04 $Å^2$).

Discussion

Potent and Selective CYP2J2 Inhibitors Have Been Identified as Useful Tools for Studying CYP2J2-related Drug Metabolism. Given the increasingly more important role CYP2J2 may play in drug metabolism and intestinal drug-drug interaction, it is necessary to expand the collection of limited number of CYP2J2 inhibitors either as useful tools to study CYP2J2 related DDI in vivo and/or as drugs for which potential DDI should be considered when they are simultaneously used with other compounds metabolized mainly by CYP2J2. In this study we set out to screen a small library of 69 marketed drugs from a range of therapeutic areas including cardiovascular, central nervous system (CNS), anti-infective, and anti-inflammatory. Among these 69 screened drugs, 8 of them have been previously studied for their inhibitory activity against CYP2J2 (Lee et al., 2012). By plotting our IC50 data for those 8 compounds against the literature data (measured by the activity remaining at a single concentration of 30 μM), it is found that those data correlate very well (R^2 = 0.97) (Figure 7). Furthermore,

telmisartan and flunarizine were identified as the most potent CYP2J2 inhibitors with K_i values of 0.19 and 0.13 μM, respectively, with over 10-fold selectivity against all five major CYP metabolic enzymes. Norfloxacin (IC50 = 2.56 μM) and metoprolol (IC50 = 4.87 μM) as highly selective CYP2J2 inhibitors with greater than 50 μM IC50s against all five major CYPs albeit their moderate inhibition activity against CYP2J2. Moreover, both telmisartan and flunarizine show no time-dependent inhibition toward CYP2J2 (Figure 3). In general, this newly discovered group of potent and selective CYP2J2 inhibitors can be useful tools for studying CYP2J2-mediated drug metabolism and CYP2J2 biological functions.

Anti-hypertension Drugs Telmisartan and Flunarizine Can Be Used to Study CYP2J2-related DDI in a Clinical Setting. Drug-drug interaction can be caused due to inhibition by one drug on a particular CYP isoform that is responsible for metabolism of another molecule at both the hepatic and intestinal levels. This may cause significantly changed pharmacokinetics of the second drug which might lead to unwanted adverse effects. Therefore, knowledge on potent inhibitors of specific CYP isoforms, especially those involved in xenobiotics metabolism, is critical for the clinical use of those medicines, and is important for the discovery and development of drugs metabolized by those specific CYP isoforms. Besides at a systematic level where liver is the major organ responsible for metabolic DDI, the gastrointestinal (GI) tract is also where DDI commonly takes place mainly due to the existence of high level metabolic enzymes and high free concentration of drugs when administered orally. Though no DDIs involving CYP2J2 have been reported in the clinic so far, it is possible that CYP2J2 could be an important CYP isoform for drug interactions in the future, especially at the GI level,

DMD Fast Forward. Published on October 2, 2012 as DOI: 10.1124/dmd.112.048264
This article has not been copyedited and formatted. The final version may differ from this version.

given its predominant expression in the small intestine and its rather broad, and growing, substrate spectrum.

In this study two marketed drugs telmisartan and flunarizine are shown to be the most potent CYP2J2 inhibitors with low μM Ki values. Both telmisartan and flunarizine are commonly prescribed anti-hypertension drugs for chronic use with good tolerability and safety profiles as reported in several human studies, where telmisartan and flunarizine were dosed as high as 160 mg and 10 mg, respectively, once daily (Van Hecken et al., 1992; Stangier et al., 2000). In the case for telmisartan, at steady state the plasma maximum concentration (C_{max}) can be as high as 3 μM (1500 ng/mL), 15-fold higher than its K_i value, 0.19 μM (Young et al., 2000). Notably, in the GI tract the concentration could be even much higher. Therefore, it is conceivable that telmisartan may have CYP2J2 inhibitory effects at both intestinal and systemic levels. In the case of flunarizine albeit relatively low plasma concentration from 0.1 to 0.3 μM given 10 mg daily dose, its intestinal concentration could still be as high as several μM (Bialer, 1993), comparing to its 0.13 μM K_i value against CYP2J2. Furthermore, the absorption of flunarizine is relatively slow with T_{max} of 4 hours in human (Bialer, 1993), which indicates that the high concentration of flunarizine in the GI tract could be maintained to have a lasting inhibitory effect of CYP2J2.

Interestingly, it has been shown that telmisartan can increase the exposure of nisoldipine, a dihydropyridine calcium channel blocker, in patients with essential hypertension (Deppe et al., 2010). The mechanism for this observed drug interaction remains unclear as nisoldipine is primarily metabolized by CYP3A4 and telmisartan has no significant inhibitory effects to this CYP. Indeed, previously telmisartan was not expected to be involved in any CYP-mediated drug interactions. However, in this case

the increased exposure of nisoldipine by co-administrated telmisartan could be related to CYP2J2 inhibition. It is noted nonetheless that interaction between telmisartan and the ATP-binding cassette (ABC) transporters could also contribute to the observed DDI (Weiss et al., 2010). The most recent FDA guidance for industry on drug interaction studies also suggests to include CYP2J2 when a new drug candidate is found to be not metabolized by the major CYPs (US Department of Health and Human Services, 2012). Under the circumstances, attention should be paid on the DDI potentials for both telmisartan and flunarizine with future co-administered compounds when the metabolism and elimination of these compounds are mainly mediated by CYP2J2. Also, both telmisartan and flunarizine can be potentially used as tool drugs to assess clinically relevant metabolic DDI related to CYP2J2.

Telmisartan and Flunarizine Are the First Discovered Non-substrate Inhibitor for CYP2J2. Ideally, the inhibitor that is used as a tool to study a CYP isoform should not be the substrate of that specific CYP enzyme; otherwise, to the least it would add complexity in experimental design. For example, one has to be very careful during the course of the experiment to ensure that the reaction time is short enough so that the degradation of such inhibitor due to metabolism is less than 20%. On the other hand, this often limits the formation of the metabolite to the extent that it is difficult to be detected by routine LC/MS equipment and therefore restricts the application of such inhibitors. In the case of CYP2J2, all the previously known potent inhibitors are also CYP2J2 substrates (Lafite et al., 2007; Lee et al., 2012). Inspired by the structural model that telmisartan binds to a pocket that is distant to the CYP2J2 catalytic center and may inhibit CYP2J2 by blocking substrate entrance and/or product egress (Figure 8, panel A), we hypothesized that telmisartan might not be a substrate to CYP2J2. This was

subsequently confirmed by the experimental data that telmisartan is not metabolized after being incubated with the recombinant CYP2J2 for 30 minutes (Figure 2). Similarly, we subjected flunarizine to the same experimental procedure and determined that it is also not a substrate of CYP2J2 (Figure 2). It is therefore for the first time that the newly discovered potent and selective CYP2J2 inhibitors are not a substrate of the enzyme. In addition, as shown above in HLM telmisartan is nearly completely not metabolized and flunarizine is only marginally metabolized; these findings are in line with the literature reports (Bialer, 1993; Deppe et al., 2010). Therefore, using these non-substrate CYP2J2 inhibitors that are also metabolically stable in human liver microsome, both telmisartan and flunarizine can be invaluable tools for studying CYP2J2 in drug metabolism and disposition in different experimental settings.

In order to evaluate the participation of CYP2J2 in drug metabolism in human liver microsome using telmisartan and/or flunarizine, it is important to identify a suitable concentration for both compounds that is able to achieve sufficient CYP2J2 inhibition while at the same time generates limited inhibition toward other major metabolizing CYPs. Given their K_i values, namely 0.19 μM for telmisartan and 0.13 μM for flunarizine, and their selectivity profiles (Table 3), it is therefore suggested that a concentration range of 1 to 2 μM for telmisartan and 0.5 to 2 μM for flunarizine—at least 4 times the respective K_i values (Suzuki et al., 2002)—may be suitable for assessing metabolism by CYP2J2 in human liver microsome system.

Telmisartan and Flunarizine Show Different CYP2J2 Inhibition Mechanisms. As discussed above based on CYP2J2 enzyme kinetics studies, telmisartan and flunarizine exhibit two distinctive inhibition mechanisms; specifically, flunarizine inhibits the enzyme by directly competing with the substrate while telmisartan is an

allosteric CYP2J2 inhibitor. In the structural models, as shown in Figure 8, panel B, flunarizine occupies the same catalytic binding site of CYP2J2 as the substrate astemizole, where it makes interactions with both the heme moiety and residues on the long helix I that are close to the catalytic center. Furthermore, the F atom on flunarizine is very close to the heme catalytic Fe atom (the distance is 3.3 Å) and in the same location where the astemizole methoxy group is, which is known to undergo demethylation metabolism catalyzed by CYP2J2. This structural model is consistent with the fact that flunarizine is not a substrate of CYP2J2 as the F atom that is close to the heme is generally metabolically inert. In fact, introducing F atoms into a small molecule is a well-known strategy in lead optimization to improve metabolic stability. Therefore, it is plausible that flunarizine not only competes the substrate at the binding site with astemizole but also at the catalytic center for reaction.

On the other hand, telmisartan binds to CYP2J2 in a grossly different fashion compared to flunarizine. Though both drugs have interactions with a limited number of overlapping CYP2J2 residues, primarily those from N-terminal loop and helix A, sheet β4 and associate loop, as well as K/β1-4 segment, there are significant differences. Specifically, telmisartan has extensive interactions with the F/G segment, particularly helix F', but is nowhere near the catalytic heme and helix I; on the contrary, as discussed above flunarizine is in close contact with both heme and helix I but has no interactions with the F/G segment (Figure 8, panel A). It has been widely suggested that the F/G segment and the B/C segment in mammalian cytochrome P450s are the most flexible parts and likely constitute the gates for substrate entrance and/or product egress paths that are necessary to gain access to the active site heme (Otyepka et al., 2007). Given that and the binding mode of telmisartan, we suggest that telmisartan might inhibit CYP2J2

activity by restraining the flexible F/G segment and thereby blocking substrate entrance and/or product egress rather than directly competing with the substrate. Limited overlaps between the telmisartan and the substrate astemizole binding regions within the CYP2J2 protein are also observed (Figure 8). Those structural observations corroborate well with the kinetics data that telmisartan is an allosteric inhibitor of CYP2J2 enzyme.

In conclusion, in this report we have discovered for the first time a number of marketed drugs, including telmisartan and flunarizine, as potent, selective, and non-substrate CYP2J2 inhibitor. Our enzyme kinetics and computer modeling studies have also elucidated their inhibition mechanisms on a molecular level that telmisartan is an allosteric CYP2J2 inhibitor while flunarizine is a direct substrate competitor. Given our increasing understanding of CYP2J2's role in drug metabolism, these newly discovered inhibitors can be potentially used as tools to study CYP2J2 in drug metabolism, particularly involving drug-drug interaction, and its biological functions.

Acknowledgements

We thank Christoph Funk and Wanping Geng from Non-Clinical Safety, Roche Pharma Research and Early Development for critical reading of the manuscript and Jian Xin, Hongxia Qiu, and Sheng Zhong from Non-Clinical Safety, Roche Pharma Research and Early Development China for helpful discussion on study design.

Authorship Contribution

Participated in research design: Ren, Yan, Fei, and Chen

Conducted experiments: Ren and Zeng

Contributed new reagents or analytic tools: Ren

Performed data analysis: Ren and Zeng

Wrote or contributed to the writing of the manuscript: Ren, Yan, Zeng, Mei, Zhang, Fei, and Chen

References

Baron A, Frieden M, and Bény JL (1997) Epoxyeicosatrienoic acids activate a high-conductance, Ca(2+)-dependent K+ channel on pig coronary artery endothelial cells. *J Physiol* **504:** 537-543.

Batsanov SS (2001) van der Waals radii of elements. *Inorg Mater* **37:** 871-885.

Bayly CI, Cieplak P, Cornell W, and Kollman PA (1993) A well-behaved electrostatic potential based method using charge restraints for deriving atomic charges: the RESP model. *J Phys Chem* **97:** 10269–10280.

Berry LM and Zhao Z (2008) An examination of IC50 and IC50-shift experiments in assessing time-dependent inhibition of CYP3A4, CYP2D6 and CYP2C9 in human liver microsomes. *Drug Metab Lett* **2:** 51-59.

Bialer M (1993) Comparative pharmacokinetics of the newer antiepileptic drugs. *Clin Pharmacokinet* **24:** 441-452.

Bondi A (1964) van der Waals volumes and radii. *J Phys Chem* **68:** 441–451.

Brash AR (2010) Arachidonic acid as a bioactive molecule. *J Clin Invest* **107:** 1339-1345.

Capdevila JH, Falck JR, and Harris RC (2000) Cytochrome P450 and arachidonic acid bioactivation. Molecular and functional properties of the arachidonate monooxygenase. *J Lipid Res* **41:** 163-181.

Case DA, Cheatham TE, III, Darden T, Gohlke H, Luo R, Merz KM, Jr, Onufriev A, Simmerling C, Wang B, and Woods RJ (2005) The AMBER biomolecular simulation programs. *J Comput Chem* **26:** 1668-1688.

Chen C, Li G, Liao W, Wu J, Liu L, Ma D, Zhou J, Elbekai RH, Edin ML, Zeldin DC, and Wang DW (2009) Selective inhibitors of CYP2J2 related to terfenadine exhibit strong activity against human cancers in vitro and in vivo. *J Pharmacol Exp Ther* **329:** 908-918.

Chen C, Wei X, Rao X, Wu J, Yang S, Chen F, Ma D, Zhou J, Dackor RT, Zeldin DC, and Wang DW (2011) Cytochrome P450 2J2 is highly expressed in hematologic malignant diseases and promotes tumor cell growth. *J Pharmacol Exp Ther* **336:** 344-355.

Connolly ML (1983) The contribution of halogen atoms to protein-ligand interactions. *J Appl Crystallogr* **16:** 548-558.

Darden T, York D, and Pedersen L (1993) Particle mesh Ewald: an *N*.log(*N*) method for Ewald sums in large systems. *J Chem Phys* **98:** 10089-10092.

Delozier TC, Kissling GE, Coulter SJ, Dai D, Foley JF, Bradbury JA, Murphy E, Steenbergen C, Zeldin DC, and Goldstein JA (2007) Detection of human CYP2C8, CYP2C9, and CYP2J2 in cardiovascular tissues. *Drug Metab Dispos* **35:** 682-688.

Deppe S, Böger RH, Weiss J, and Benndorf RA (2010) Telmisartan: a review of its pharmacodynamic and pharmacokinetic properties. *Expert Opin Drug Metab Toxicol* **6:** 863-710.

Ding X and Kaminsky LS (2003) Human extrahepatic cytochromes P450: function in xenobiotic metabolism and tissue-selective chemical toxicity in the respiratory and gastrointestinal tracts. *Annu Rev Pharmacol Toxicol* **43:** 149-173.

Fleming I (2004) Cytochrome P450 epoxygenases as EDHF synthase(s). . *Pharmacol Res* **49:** 525-533.

Freedman RS, Wang E, Voiculescu S, Patenia R, Bassett RL, Jr, Deavers M, Marincola FM, Yang P, and Newman RA (2007) Comparative analysis of peritoneum and tumor eicosanoids and pathways in advanced ovarian cancer. *Clin Cancer Res* **13:** 5736-5744.

Friesner RA, Banks JL, Murphy RB, Halgren TA, Klicic JJ, Mainz DT, Repasky MP, Knoll EH, Shaw DE, Shelley M, Perry JK, Francis P, and Shenkin PS (2004) Glide: a new approach for rapid, accurate docking and scoring. 1. Method and assessment of docking accuracy. *J Med Chem* **47:** 1739-1749.

Frisch MJ, Trucks GW, Schlegel HB, Scuseria GE, Robb MA, Cheeseman JR, Scalmani G, Barone V, Mennucci B, Petersson GA, Nakatsuji H, Caricato M, Li X, Hratchian HP, Izmaylov AF, Bloino J, Zheng G, Sonnenberg JL, Hada M, Ehara M, Toyota K, Fukuda R, Hasegawa J, Ishida M, Nakajima T, Honda Y, Kitao O, Nakai H, Vreven T, Montgomery JA, Jr, Peralta JE, Ogliaro F, Bearpark M, Heyd JJ, Brothers E, Kudin KN, Staroverov VN, Kobayashi R, Normand J, Raghavachari K, Rendell A, Burant JC, Iyengar SS, Tomasi J, Cossi M, Rega N, Millam NJ, Klene M, Knox JE, Cross JB, Bakken V, Adamo C, Jaramillo J, Gomperts R, Stratmann RE, Yazyev O, Austin AJ, Cammi R, Pomelli C, Ochterski JW, Martin RL, Morokuma K, Zakrzewski VG, Voth GA, Salvador P, Dannenberg JJ, Dapprich S, Daniels AD, Farkas Ö, Foresman JB, Ortiz JV, Cioslowski J, and Fox DJ (2009) *Gaussian 09, Revision A.1*. Gaussian, Inc., Wallingford, CT.

Giammona DA (1984) Ph.D. thesis: An examination of conformational flexibility in porphyrin and bulky-ligand binding in myoglobin, University of California, Davis.

Guengerich FP and Rendic S (2010) Update information on drug metabolism systems - 2009, part I. *Curr Drug Metab* **11:** 1-3.

Halgren TA, Murphy RB, Friesner RA, Beard HS, Frye LL, Pollard WT, and Banks JL (2004) Glide: a new approach for rapid, accurate docking and scoring. 2. Enrichment factors in database screening. *J Med Chem* **47:** 1750-1759.

Hashizume T, Imaoka S, Mise M, Terauchi Y, Fujii T, Miyazaki H, Kamataki T, and Funae Y (2002) Involvement of CYP2J2 and CYP4F12 in the metabolism of ebastine in human intestinal microsomes. *J Pharmacol Exp Ther* **300:** 298-304.

Imig JD, Inscho EW, Deichmann PC, Reddy KM, and Falck JR (1999) Afferent arteriolar vasodilation to the sulfonimide analog of 11,12-epoxyeicosatrienoic acid involves protein kinase A. *Hypertension* **33:** 408-413.

Jiang JG, Chen CL, Card JW, Yang S, Chen JX, Fu XN, Ning YG, Xiao X, Zeldin DC, and Wang DW (2005) Cytochrome P450 2J2 promotes the neoplastic phenotype of carcinoma cells and is up-regulated in human tumors. *Cancer Res* **65:** 4707-4715.

Jiang JG, Ning YG, Chen C, Ma D, Liu ZJ, Yang S, Zhou J, Xiao X, Zhang XA, Edin ML, Card JW, Wang J, Zeldin DC, and Wang DW (2007) Cytochrome p450 epoxygenase promotes human cancer metastasis. *Cancer Res* **67:** 6665-6674.

Jorgensen WL, Chandrasekhar J, Madura JD, Impey RW, and Klein ML (1983) Comparison of simple potential functions for simulating liquid water. *J Chem Phys* **79:** 926-935.

Lafite P, Dijols S, Zeldin DC, Dansette PM, and Mansuy D (2007) Selective, competitive and mechanism-based inhibitors of human cytochrome P450 2J2. *Arch Biochem Biophys* **464:** 155-168.

Larsen BT, Miura H, Hatoum OA, Campbell WB, Hammock BD, Zeldin DC, Falck JR, and Gutterman DD (2006) Epoxyeicosatrienoic and dihydroxyeicosatrienoic acids dilate human coronary arterioles via BK(Ca) channels: implications for soluble epoxide hydrolase inhibition. *Am J Physiol Heart Circ Physiol* **290:** 491-499.

Lee CA, Jones JPI, Katayama J, Kaspera R, Jiang Y, Freiwald S, Smith E, Walker GS, and Totah RA (2012) Identifying a selective substrate and inhibitor pair for the evaluation of CYP2J2 activity. *Drug Metab Dispos* **40:** 943-951.

Lee CA, Neul D, Clouser-Roche A, Dalvie D, Wester MR, Jiang Y, Jones JP, III, Freiwald S, Zientek M, and Totah RA (2010) Identification of novel substrates for human cytochrome P450 2J2. *Drug Metab Dispos* **38:** 347-356.

Li W, Tang Y, Liu H, Cheng J, Zhu W, and Jiang H (2008) Probing ligand binding modes of human cytochrome P450 2J2 by homology modeling, molecular dynamics simulation, and flexible molecular docking. *Proteins* **71:** 938-949.

Liu KH, Kim MG, Lee DJ, Yoon YJ, Kim MJ, Shon JH, Choi CS, Choi YK, Desta Z, and Shin JG (2006) Characterization of ebastine, hydroxyebastine, and carebastine metabolism by human liver microsomes and expressed cytochrome P450 enzymes: major roles for CYP2J2 and CYP3A. *Drug Metab Dispos* **34:** 1793-1797.

Matsumoto S, Hirama T, Matsubara T, Nagata K, and Yamazoe Y (2002) Involvement of CYP2J2 on the intestinal first-pass metabolism of antihistamine drug, astemizole. *Drug Metab Dispos* **30:** 1240-1245.

Matsumoto S and Yamazoe Y (2001) Involvement of multiple human cytochromes P450 in the liver microsomal metabolism of astemizole and a comparison with terfenadine. *Br J Clin Pharmacol* **51:** 133-142.

Miyamoto S and Kollman PA (1992) Settle: An analytical version of the SHAKE and RATTLE algorithm for rigid water models. *J Comput Chem* **13:** 952–962.

Node K, Huo Y, Ruan X, Yang B, Spiecker M, Ley K, Zeldin DC, and Liao JK (1996) Anti-inflammatory properties of cytochrome P450 epoxygenase-derived eicosanoids. *Science* **285:** 1276-1279.

Oliw EH (1994) Oxygenation of polyunsaturated fatty acids by cytochrome P450 monooxygenases. *Prog Lipid Res* **33:** 329-354.

Onufriev A, Bashford D, and Case DA (2000) Modification of the generalized Born model suitable for macromolecules. *J Phys Chem B* **104:** 3712–3720.

Otyepka M, Skopalík J, Anzenbacherová E, and Anzenbacher P (2007) What common structural features and variations of mammalian P450s are known to date? *Biochim Biophys Acta* **1770:** 376-389.

Paine MF, Hart HL, Ludington SS, Haining RL, Rettie AE, and Zeldin DC (2006) The human intestinal cytochrome P450 "pie". *Drug Metab Dispos* **34:** 880-886.

Pastor RW, Brooks BR, and Szabo A (1998) An analysis of the accuracy of Langevin and molecular dynamics algorithms. *Mol Phys* **65:** 1409-1419.

Qiu D, Shenkin PS, Hollinger FP, and Still WC (1997) The GB/SA continuum model for solvation. A fast analytical method for the calculation of approximate Born radii. *J Phys Chem* **101:** 3005–3014.

Seubert J, Yang B, Bradbury JA, Graves J, Degraff LM, Gabel S, Gooch R, Foley J, Newman J, Mao L, Rockman HA, Hammock BD, Murphy E, and Zeldin DC (2004) Enhanced postischemic functional recovery in CYP2J2 transgenic hearts involves mitochondrial ATP-sensitive K+ channels and p42/p44 MAPK pathway. *Circ Res* **95:** 506-514.

Stangier J, Su CA, and Roth W (2000) Pharmacokinetics of orally and intravenously administered telmisartan in healthy young and elderly volunteers and in hypertensive patients. *J Int Med Res* **28:** 149-167.

Suzuki H, Kneller MB, Haining RL, Trager WF, and Rettie AE (2002) (+)-N-3-Benzyl-nirvanol and (-)-N-3-benzyl-phenobarbital: new potent and selective in vitro inhibitors of CYP2C19. *Drug Metab Dispos* **30:** 235-239.

Testino SA, Jr and Patonay G (2003) High-throughput inhibition screening of major human cytochrome P450 enzymes using an in vitro cocktail and liquid chromatography-tandem mass spectrometry. *J Pharm Biomed Anal* **30:** 1459-1467.

US Department of Health and Human Services, Food and Drug Administration (FDA), Center for Drug Evaluation and Research (CDER), Center for Biologics Evaluation and Research (CBER) (2012) Guidance for Industry. Drug Interaction Studies - Study Design, Data Analysis, Implications for Dosing, and Labeling Recommendations.

Van Hecken AM, Depré M, De Schepper PJ, Fowler PA, Lacey LF, and Durham JM (1992) Lack of effect of flunarizine on the pharmacokinetics and pharmacodynamics of sumatriptan in healthy volunteers. *Br J Clin Pharmacol* **34:** 82-84.

Walsky RL and Obach RS (2004) Validated assays for human cytochrome P450 activities. *Drug Metab Dispos* **32:** 647-660.

Wang J, Wolf RM, Caldwell JW, Kollamn PA, and Case DA (2004) Development and testing of a general amber force field. *J Comput Chem* **25:** 1157-1174.

Weaver R, Graham KS, Beattie IG, and Riley RJ (2003) Cytochrome P450 inhibition using recombinant proteins and mass spectrometry/multiple reaction monitoring technology in a cassette incubation. *Drug Metab Dispos* **31:** 955-966.

Weiser J, Shenkin PS, and Still WC (1999) Approximate atomic surfaces from linear combinations of pairwise overlaps (LCPO). *J Comput Chem* **20:** 217–230.

Weiss J, Sauer A, Divac N, Herzog M, Schwedhelm E, Böger RH, Haefeli WE, and Benndorf RA (2010) Interaction of angiotensin receptor type 1 blockers with ATP-binding cassette transporters. *Biopharm Drug Dispos* **31:** 150-161.

Wu S, Moomaw CR, Tomer KB, Falck JR, and Zeldin DC (1996) Molecular cloning and expression of CYP2J2, a human cytochrome P450 arachidonic acid epoxygenase highly expressed in heart. *J Biol Chem* **271:** 3460-3468.

Xiao B, Li X, Yan J, Yu X, Yang G, Xiao X, Voltz JW, Zeldin DC, and Wang DW (2010) Overexpression of cytochrome P450 epoxygenases prevents development of hypertension in spontaneously hypertensive rats by enhancing atrial natriuretic peptide. *J Pharmacol Exp Ther* **334:** 784-794.

Xu X, Zhang XA, and Wang DW (2011) The roles of CYP450 epoxygenases and metabolites, epoxyeicosatrienoic acids, in cardiovascular and malignant diseases. *Adv Drug Deliv Rev* **63:** 597-609.

Young CL, Dias VC, and Stangier J (2000) Multiple-dose pharmacokinetics of telmisartan and of hydrochlorothiazide following concurrent administration in healthy subjects. *J Clin Pharmacol* **40:** 1323-1330.

Footnotes

This work was supported by National Key Project [Grants 2010CB945501, 2010CB912604]; National Science Foundation of China [Grant 21173082]; Shanghai Rising-Star Program [Grant 11QA1402000]; National Natural Science Foundation of China [Grants 10974054, 20933002]; and Shanghai Pujiang Program [Grant 09PJ1404000].

Figure Legends

FIGURE 1. Representative IC50 plots for telmisartan (A) and flunarizine (B) inhibition of astemizole *O*-demethylation using recombinant CYP2J2 with astemizole concentrations from 0.1 to 20 μM.

FIGURE 2. Disappearance of astemizole (A), telmisartan (B), and flunarizine (C) measured from incubation with recombinant CYP2J2 in the presence of NADPH at different time points (n = 2).

FIGURE 3. IC50 determination of inhibition of CYP2J2-mediated astemizole *O*-demethylation by telmisartan (A) and flunarizine (B) in the presence and absence of NADPH. The inhibitors were pre-incubated with CYP2J2 for 30 minutes. The IC50 shift was calculated as IC50 in the absence of NADPH over IC50 in the presence of NADPH in order to evaluate time-dependent inhibition.

FIGURE 4. Inhibition assay against the enzymatic activity of recombinant CYP2J2. Non-linear regression of the initial velocity at various substrate concentrations under the presence of telmisartan (A) and flunarizine (B) as the inhibitor with concentrations from 0.1 to 2 μM and from 0.2 to 5 μM, respectively. Dixon plots with amplified insets for the enzyme kinetic study of CYP2J2-mediated astemizole *O*-demethylation in the presence of different concentrations of telmisartan (C) and flunarizine (D) as the inhibitor. Astemizole concentrations used were 0.05 (●), 0.1 (□), 0.15 (▲), 0.3 (◇), and 0.45 μM

(▽) (n = 4). The replots of the slope of Dixon plot versus reciprocal of substrate concentration for telmisartan (E) and flunarizine (F).

FIGURE 5. Initial docking model of the CYP2J2 complex with (A) telmisartan and (B) flunarizine. The CYP2J2 protein is in cartoon representation and colored in rainbow spectrum; the heme and the inhibitor are in stick and colored in orange and yellow, respectively. The root-mean-square deviations (RMSDs) for CYP2J2–telmisartan (C) and CYP2J2–flunarizine (D) complexes over the 2 ns MD simulation. The RMSDs were computed relative to the respective starting structures. The top panel is for the entire complex, middle panel for the heme alone, and the bottom panel is for the inhibitor. The minimum fluctuation in the RMSD value indicates the CYP2J2 protein displays limited overall conformational change in both systems.

FIGURE 6. CYP2J2 inhibitor binding pocket at the end of the 2 ns MD simulation for telmisartan (A) and flunarizine (B). The pocket for telmisartan (A, C) is largely comprised of residues of hydrophobic nature, mainly from N-terminal loop and helix A (Val59, Phe61, Ser64, His65, and Val68), sheet β1 and associated loops (Leu83, Ile86, and Met400), helix K' (Asn404 and Thr406), sheet β4 and associate loop (Arg484, Gly486, and Ile487), K/β1-4 segment (Ile376, Pro377, Leu378, Val380, and Pro381), B/C segment (Val113, Thr114, Met116, and Arg117), helix F (Glu222), as well as F/G segment (Gln228, Asn231, and Val232). The binding pocket for flunarizine (B, D) is formed primarily by hydrophobic residues, largely from N-terminal loop and helix A (Gln63, Ser64, and His65), sheet β4 and associate loop (Arg484 and Ile487), K/β1-4

segment (Ile376, Pro377, Leu378, Asn379, Val380, and Pro381), B/C segment (Pro112, Val113, Thr114, Arg117, and Ile127), helix F (Glu222), as well as helix I (Phe310, Ala311, and Thr315) and the heme porphyrin ring. The CYP2J2 protein is in cartoon representation and colored in rainbow spectrum; the heme is in stick and colored in orange; the protein residues that are within 4 Å of the inhibitor are shown in stick and colored in rainbow spectrum; inhibitors are in stick and colored in yellow (telmisartan) and magenta (flunarizine), respectively. The 2D representation of the inhibitor binding pocket for telmisartan (C) and flunarizine (D). The inhibitor physicochemical properties are also shown.

FIGURE 7. Comparison of measured compound CYP2J2 inhibitory activities (IC50) with those reported in the literature (% activity remaining). Astemizole *O*-demethylation was used for evaluating the metabolic activity of CYP2J2; compounds with a measured IC50 value higher than 50 μM in our lab were treated as IC50 = 50 μM in the comparison; percentage activity remaining was obtained at single inhibitor concentration of 30 μM as reported in the literature and only compounds with activity remaining less than 100% were included. Compounds included were amodiaquine, nicardipine, haloperidol, clozapine, lansoprazole, verapamil, fluoxetine, and omeprazole.

FIGURE 8. Overlay of substrate (astemizole) and the inhibitor within the binding pocket of CYP2J2 for telmisartan (A) and flunarizine (B), respectively. The CYP2J2 protein is in cartoon representation and colored in rainbow spectrum; the heme is in stick and colored in orange; telmisartan, flunarizine, and astemizole are in stick and colored in yellow, magenta, and green, respectively.

DMD Fast Forward. Published on October 2, 2012 as DOI: 10.1124/dmd.112.048264
This article has not been copyedited and formatted. The final version may differ from this version.

Table 1: Compounds investigated in the recombinant CYP2J2 inhibition assay.

Compound Name	Therapeutic Use	Compound Name	Therapeutic Use	Compound Name	Therapeutic Use
Acetaminophen	CNS	Erythromycin	Anti-infective	Nimodipine	Cardiovascular
Acyclovir	Anti-infective	Fexofenadine	Anti-allergic	Norfloxacin	Anti-infective
Alprenolol	Cardiovascular	Flecainide	Cardiovascular	Olmesartan	Cardiovascular
Amodiaquine	Anti-infective	Flunarizine	Cardiovascular	Omeprazole	Gastrointestinal
Amoxicillin	Anti-infective	Fluoxetine	CNS	Perphenazine	CNS
Antipyrin	Anti-inflammatory	Furosemide	Cardiovascular	Phenacetin	CNS
Benzbromarone	Anti-inflammatory	Haloperidol	CNS	Piroxicam	Anti-inflammatory
Benzydamine	Anti-inflammatory	Hydrochlorothiazide	Cardiovascular	Prednisolone	Anti-inflammatory
Bepridil	Cardiovascular	Hydrocortisone	Anti-inflammatory	Probucol	Lipid Regulating
Bufuralol	Cardiovascular	Ibuprofen	Anti-inflammatory	Propafenone	Cardiovascular
Carbamazepine	CNS	Imipramine	CNS	Propranolol	Cardiovascular
Ceftriaxone	Anti-infective	Ketoprofen	Anti-inflammatory	Ranitidine	Gastrointestinal
Chlorpromazine	CNS	Lansoprazole	Gastrointestinal	Sertraline	CNS
Chlorzoxazone	CNS	Mefenamic acid	Anti-inflammatory	Sulfaphenazole	Anti-infective
Cimetidine	Gastrointestinal	Mephenytoin	CNS	Sulfasalazine	Anti-infective
Clozapine	CNS	Metoprolol	Cardiovascular	Sulpiride	CNS
Desipramine	CNS	Mexiletine	Cardiovascular	Telmisartan	Cardiovascular
Dexamethasone	Anti-inflammatory	Mibefradil	Cardiovascular	Tenoxicam	Anti-inflammatory
Dextromethorphan	CNS	Minocycline	Anti-infective	Ticlopidine	Cardiovascular
Diclofenac	Anti-inflammatory	Naloxone	CNS	Triamcinolone	Anti-inflammatory
Diltiazem	Cardiovascular	Naproxen	Anti-inflammatory	Trimethoprim	Anti-infective
Diphenhydramine	CNS	Nicardipine	Cardiovascular	Troleandomycin	Anti-infective
Eletriptan	CNS	Nifedipine	Cardiovascular	Verapamil	Cardiovascular

DMD Fast Forward. Published on October 2, 2012 as DOI: 10.1124/dmd.112.048264
This article has not been copyedited and formatted. The final version may differ from this version.

Table 2: Probe substrates, final concentrations, metabolites, and LC-MS/MS parameters for the five metabolites and internal standard (IS).

P450	Substrate	Concentration (μM)	Metabolite	MRM	CE
					eV
CYP1A2	Phenacetin	50	Acetaminophen	152.2>110.1	20
CYP2C9	Tolbutamide	150	4'-hydroxytolbutamide	287.0>188.0	20
CYP2C19	Omeprazole	10	5-hydroxyomeprazole	361.9>214.0	18
CYP2D6	Bufuralol	10	1' -hydroxybufuralol	278.0>186.0	17
CYP3A4	Testosterone	50	6β-hydroxytestosterone	305.2>269.1	20
IS	Dextrorphan	3		258.0>201.0	20

MRM: multiple reaction monitoring

CE: collision energy

DMD Fast Forward. Published on October 2, 2012 as DOI: 10.1124/dmd.112.048264
This article has not been copyedited and formatted. The final version may differ from this version.

Table 3: Inhibitory activities of tested drugs towards CYP2J2, CYP3A4, CYP2D6, CYP2C9, CYP2C19, and CYP1A2 using recombinant CYP2J2 protein and human liver microsome together with CYP isoform selective substrates.

No.	Drug Name	IC50 (μM)					
		2J2	**3A4**	**2D6**	**2C9**	**2C19**	**1A2**
1	Telmisartan	0.42 ± 0.10	>50	>50	4.78 ± 1.70	>50	>50
2	Flunarizine	0.94 ± 0.01	>50	7.89 ± 0.83	>50	>50	>50
3	Amodiaquine	0.99 ± 0.05	>50	0.64 ± 0.03	>50	>50	41.0 ± 4.45
4	Nicardipine	1.69 ± 0.35	0.38 ± 0.01	1.78 ± 0.06	0.66 ± 0.05	0.56 ± 0.23	13.3 ± 10.5
5	Mibefradil	2.14 ± 0.15	0.47 ± 0.001	0.84 ± 0.10	28.4 ± 3.38	1.32 ± 0.62	>50
6	Norfloxacin	2.56 ± 0.64	>50	>50	>50	>50	>50
7	Nifedipine	3.06 ± 0.51	5.62 ± 1.87	>50	4.08 ± 1.32	5.42 ± 1.58	2.30 ± 0.04
8	Nimodipine	3.38 ± 0.52	1.78 ± 0.77	18.3 ± 2.77	1.69 ± 0.30	2.17 ± 1.51	7.20 ± 2.76
9	Benzbromarone	4.26 ± 0.11	29.2 ± 2.18	>50	>50	18.2 ± 5.05	33.1 ± 3.25
10	Haloperidol	4.69 ± 0.47	33.1 ± 3.88	3.64 ± 1.75	>50	>50	>50
11	Metoprolol	4.87 ± 0.10	>50	>50	>50	>50	>50
12	Triamcinolone	9.47 ± 1.32	49.1± 4.24	>50	>50	>50	>50
13	Perphenazine	10.6 ± 1.22	13.9 ± 0.28	0.12 ± 0.01	21.3 ± 3.82	18.5 ± 0.71	4.49 ± 0.16
14	Bepridil	11.5 ± 0.21	23.6 ± 4.52	>50	4.31 ± 1.21	32.2 ± 5.35	>50
15	Clozapine	14.1 ± 2.97	46.3 ± 1.81	18.0 ± 6.68	21.2 ± 6.79	45.3 ± 4.81	>50
16	Sertraline	18.5 ± 1.06	13.6 ± 2.76	2.88 ± 0.03	>50	22.5 ± 2.12	29.7 ± 3.46
17	Ticlopidine	21.8 ± 1.70	32.7 ± 0.71	4.80 ± 0.83	31.1 ± 9.62	28.4 ± 3.61	8.59 ± 0.08
18	Verapamil	22.0 ± 0.28	12.0 ± 1.20	43.3 ± 1.64	>50	21.8 ± 1.06	>50
19	Chlorpromazine	24.4 ± 0.26	23.3 ± 1.91	1.49 ± 0.28	>50	34.1 ± 4.31	4.14 ± 1.11
20	Ceftriaxone	27.4 ± 10.2	>50	>50	>50	>50	>50

CYP2J2 IC50 values for all other drugs in Table 1 are above 50 μM.

DMD Fast Forward. Published on October 2, 2012 as DOI: 10.1124/dmd.112.048264
This article has not been copyedited and formatted. The final version may differ from this version.

Table 4: Binding free energy analysis of telmisartan and flunarizine to CYP2J2.

	Telmisartan	Flunarizine	Δ
ΔE_{elec}	–7.0 (7.4)	–76.0 (5.1)	69.0
ΔE_{vdW}	–69.4 (2.4)	–56.0 (2.4)	–13.4
ΔG_{GB}	30.1 (6.6)	86.8 (5.0)	–56.7
$\Delta G_{nonpolar}$	–9.4 (0.1)	–7.6 (0.1)	–1.8
$\Delta G_{solvation} = \Delta G_{GB} + \Delta G_{nonpolar}$	20.9 (6.6)	79.2 (4.9)	–58.3
$\Delta G_{elec} = \Delta G_{GB} + \Delta E_{elec}$	23.3 (2.4)	10.8 (2.0)	12.5
ΔG_{bind}	–55.5 (3.0)	–52.8 (2.4)	–2.7

All energies are in kcal/mol. Values in parentheses are standard deviations. Δ is defined as telmisartan – flunarizine. Telmisartan has a much stronger van der Waals contribution to the binding free energy (–69.4 kcal/mol) than flunarizine (–56.0 kcal/mol), while this is largely compensated by the unfavorable electrostatic contribution between the drug and CYP2J2, namely, 23.3 kcal/mol for telmisartan and 10.8 kcal/mol for flunarizine. In addition, the nonpolar contribution of the solvation free energy between the two cases is quite similar, that is, –9.4 kcal/mol for telmisartan and –7.6 kcal/mol for flunarizine.

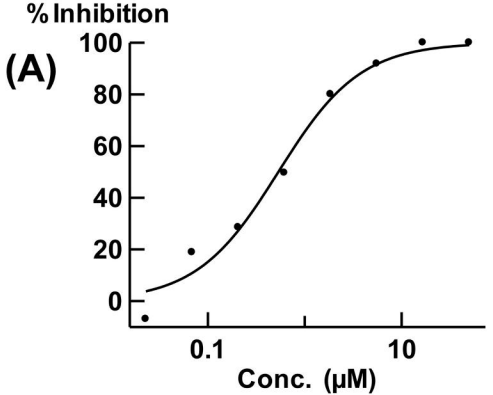
% Inhibition
(A)
100
80
60
40
20
0
0.1
10
Conc. (μM)

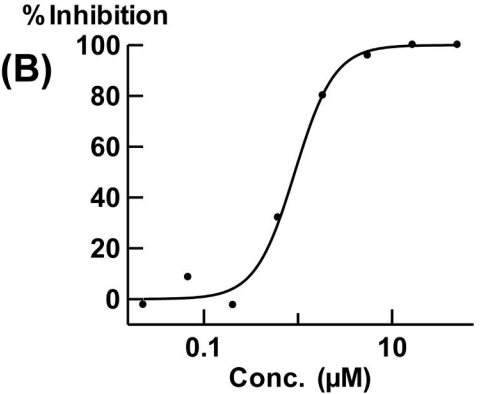
% Inhibition
(B)
100
80
60
40
20
0
0.1
10
Conc. (μM)

Figure 1

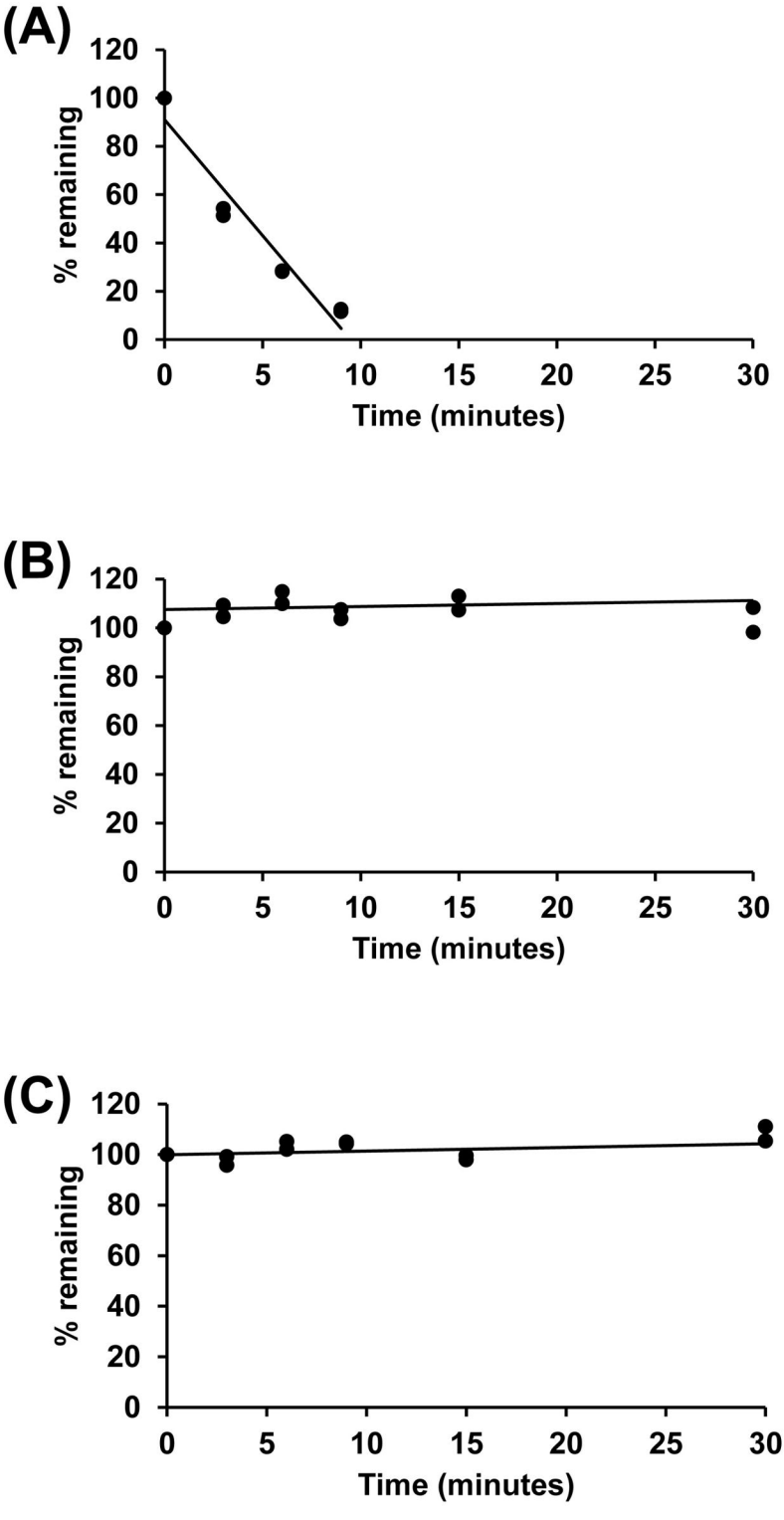
(A)
120
100
80
60
40
20
0
% remaining
0
5
10
15
20
25
30
Time (minutes)
(B)
120
100
80
60
40
20
0
% remaining
0
5
10
15
20
25
30
Time (minutes)
(C)
120
100
80
60
40
20
0
% remaining
0
5
10
15
20
25
30
Time (minutes)

Figure 2

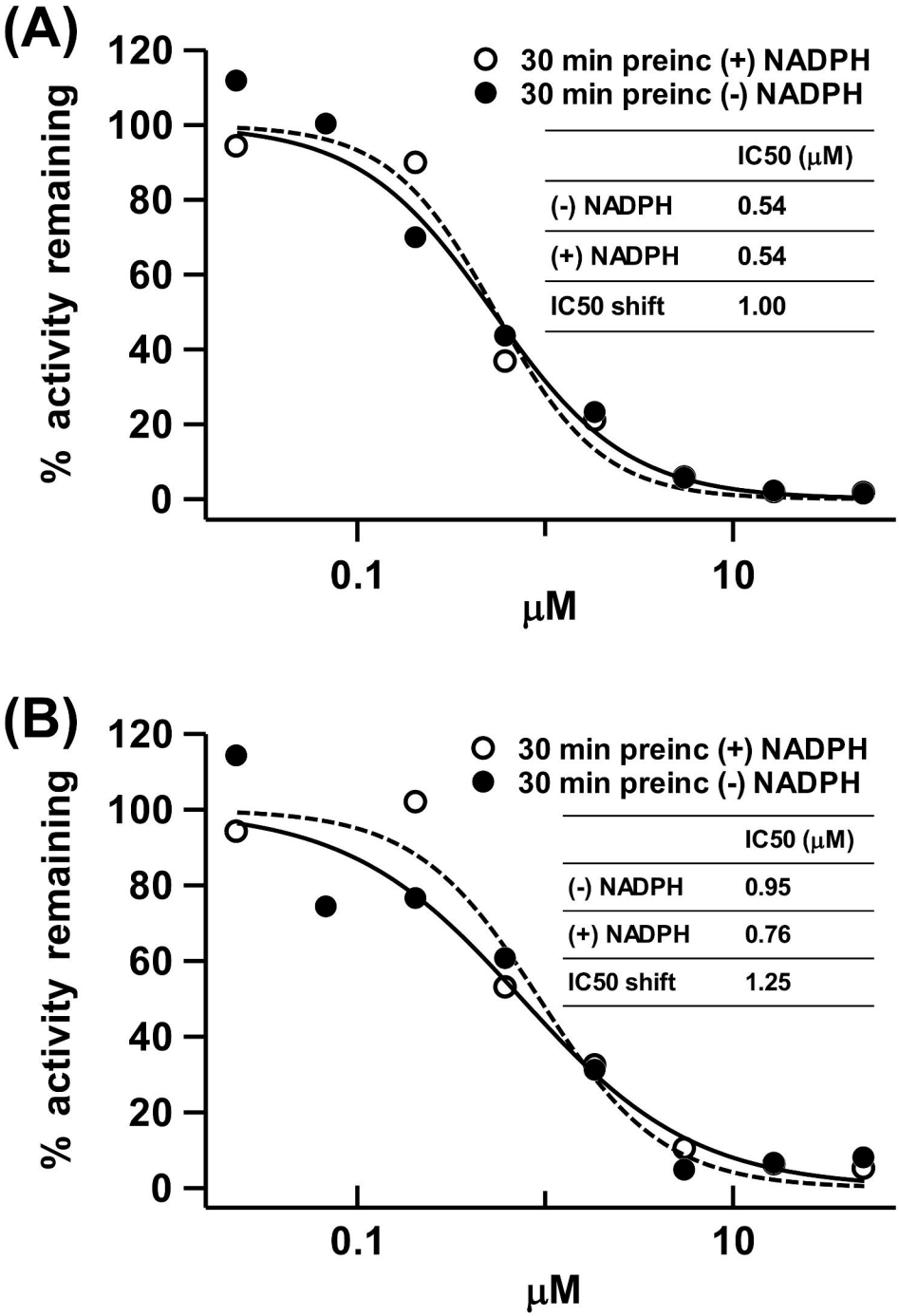
(A)
120
100
80
60
40
20
0
% activity remaining
30 min preinc (+) NADPH
30 min preinc (-) NADPH
IC50 (μM)
(-) NADPH 0.54
(+) NADPH 0.54
IC50 shift 1.00
0.1
10
μM
(B)
120
100
80
60
40
20
0
% activity remaining
30 min preinc (+) NADPH
30 min preinc (-) NADPH
IC50 (μM)
(-) NADPH 0.95
(+) NADPH 0.76
IC50 shift 1.25
0.1
10
μM

Figure 3

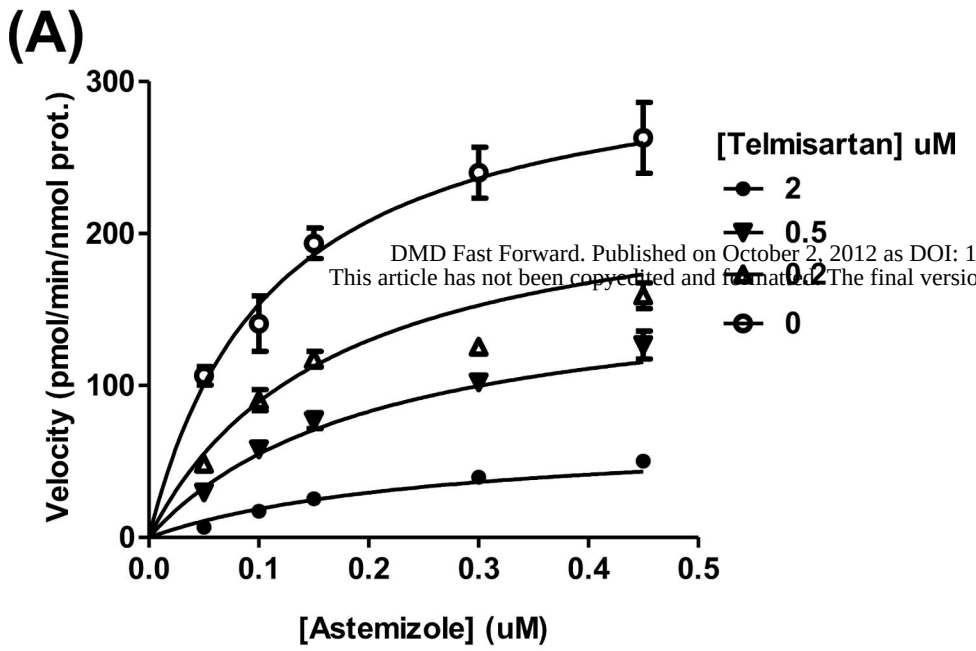

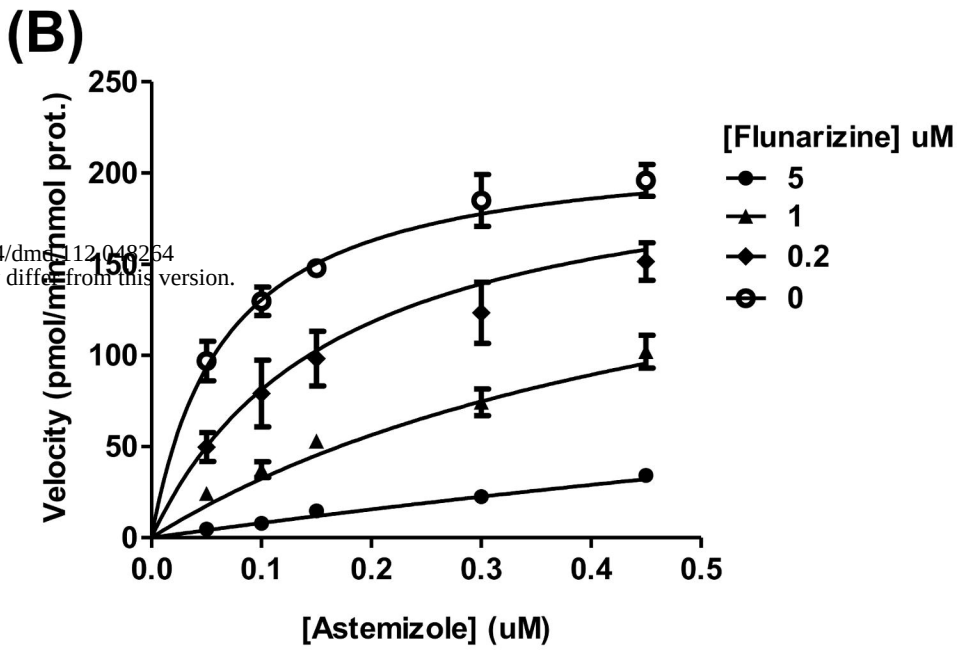

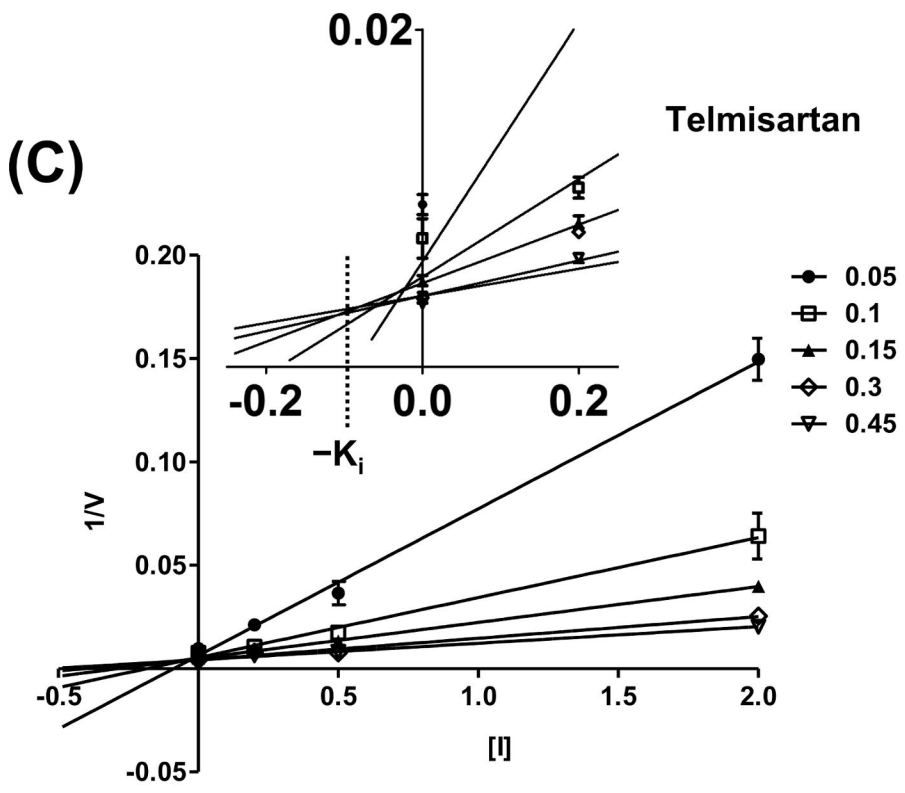

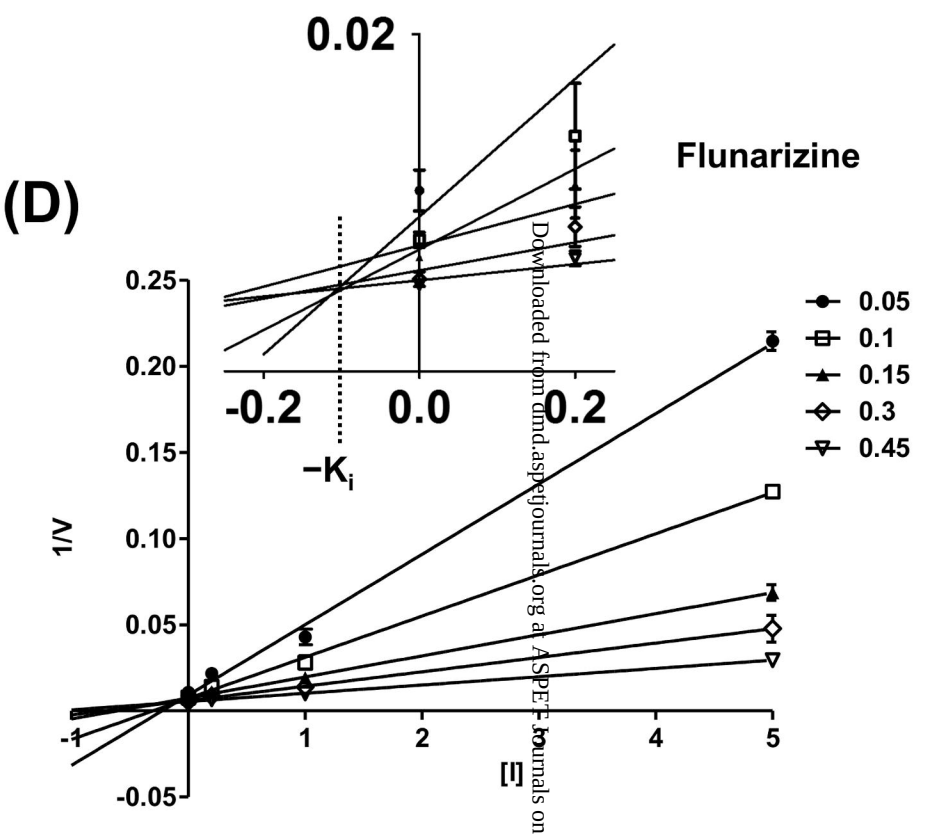

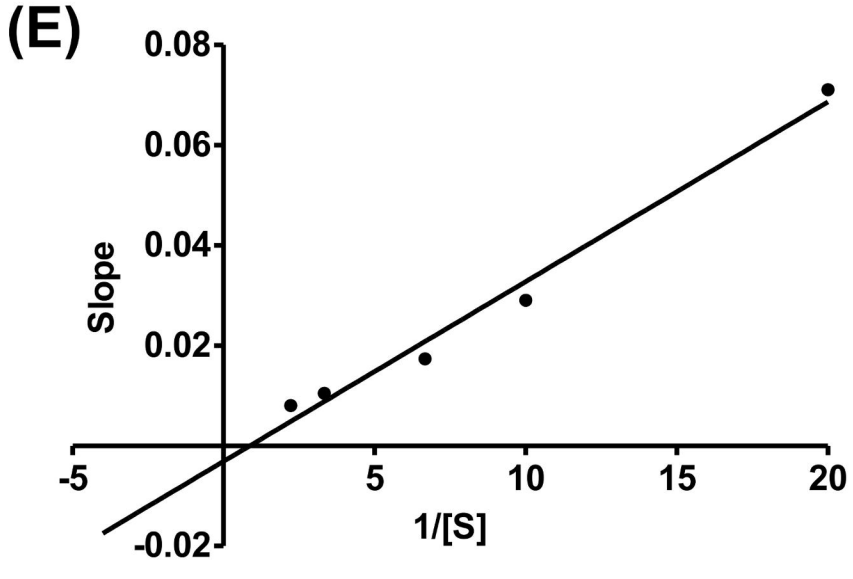

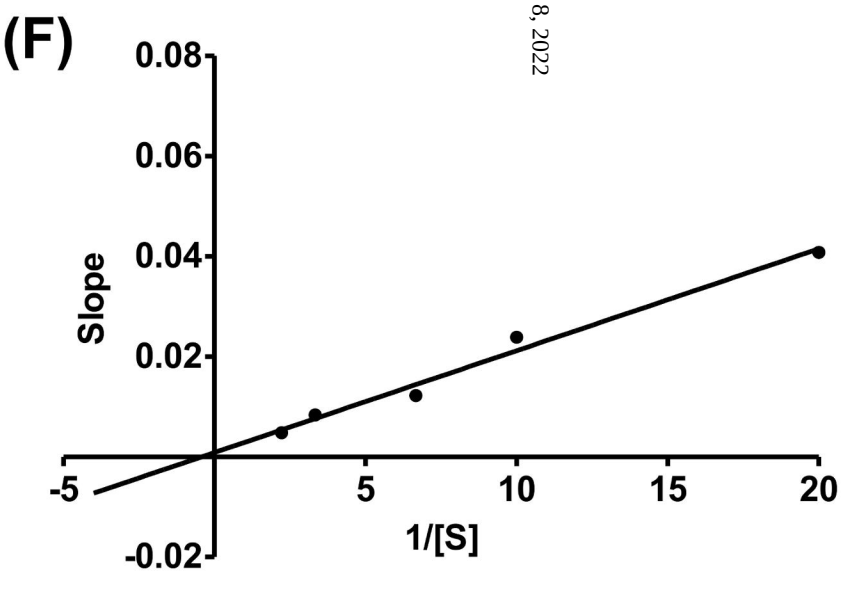

Figure 4

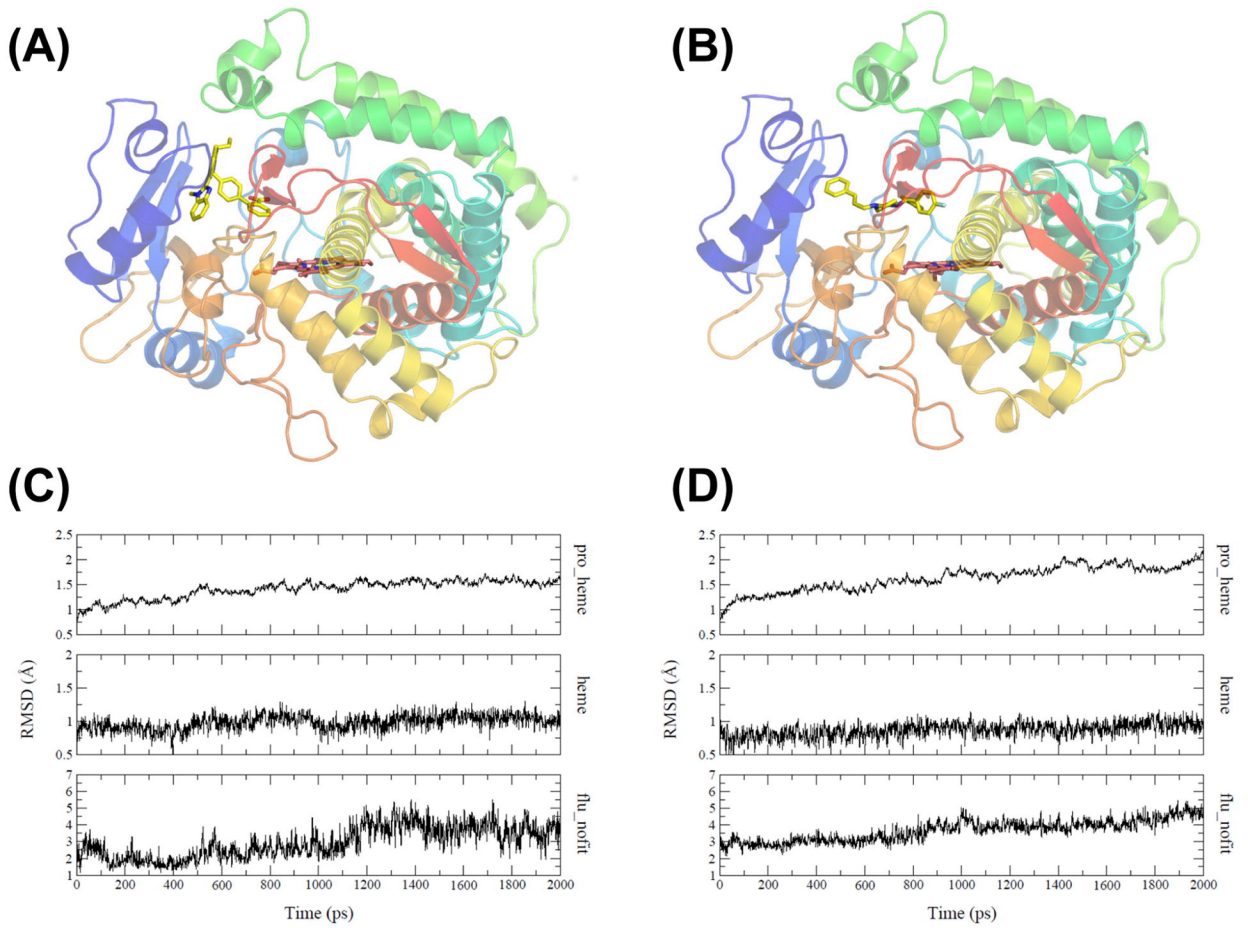

Figure 5

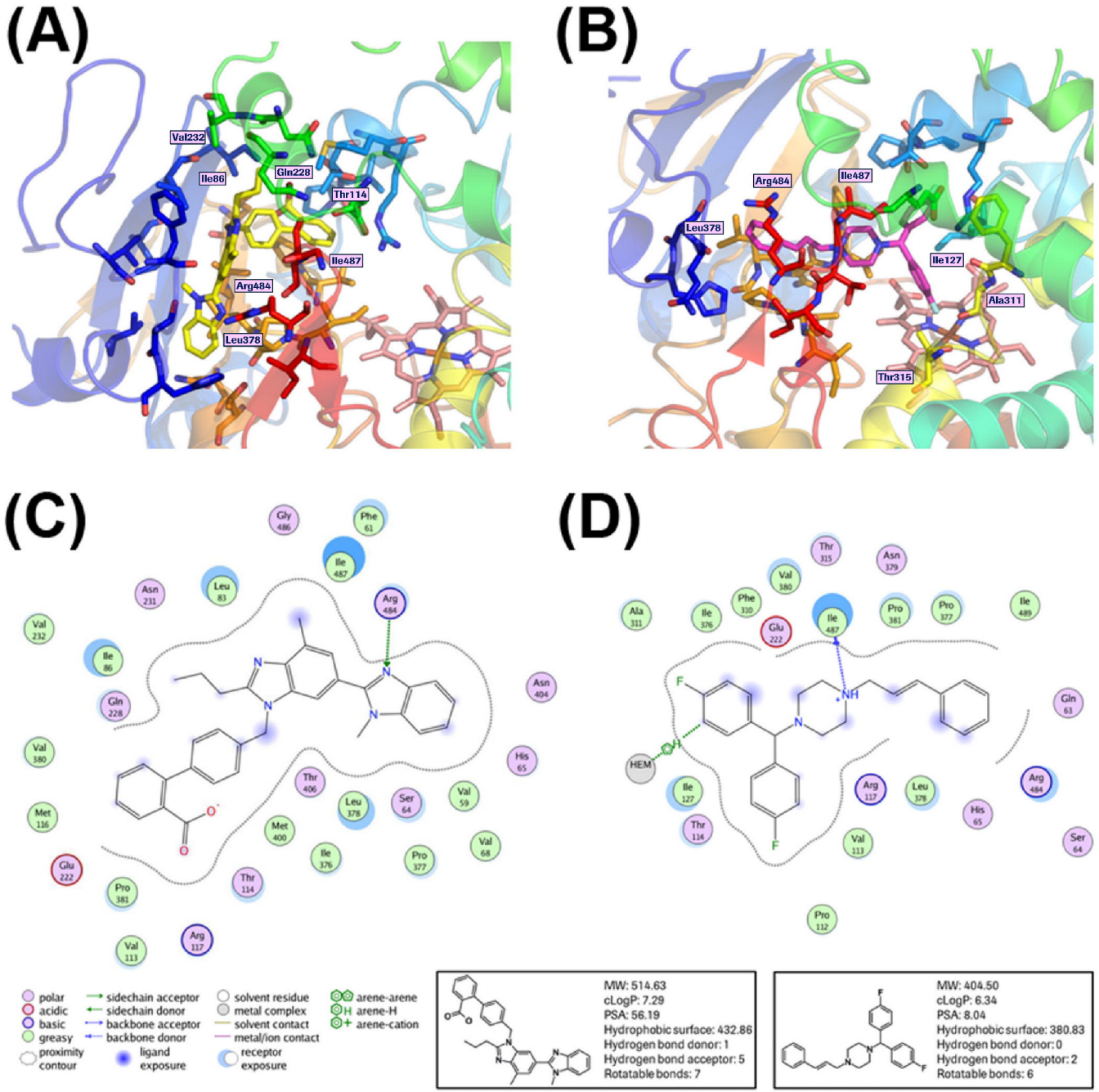
(A)
Val232
Ile86
Gln228
Thr114
Ile487
Arg484
Leu378
(B)
Arg484
Ile487
Leu378
Ile127
Ala311
Thr315
(C)
(D)
HEM
polar
acidic
basic
greasy
proximity contour
sidechain acceptor
sidechain donor
backbone acceptor
backbone donor
ligand exposure
solvent residue
metal complex
solvent contact
metal/ion contact
receptor exposure
arene-arene
arene-H
arene-cation
MW: 514.63
cLogP: 7.29
PSA: 56.19
Hydrophobic surface: 432.86
Hydrogen bond donor: 1
Hydrogen bond acceptor: 5
Rotatable bonds: 7
MW: 404.50
cLogP: 6.34
PSA: 8.04
Hydrophobic surface: 380.83
Hydrogen bond donor: 0
Hydrogen bond acceptor: 2
Rotatable bonds: 6

Figure 6

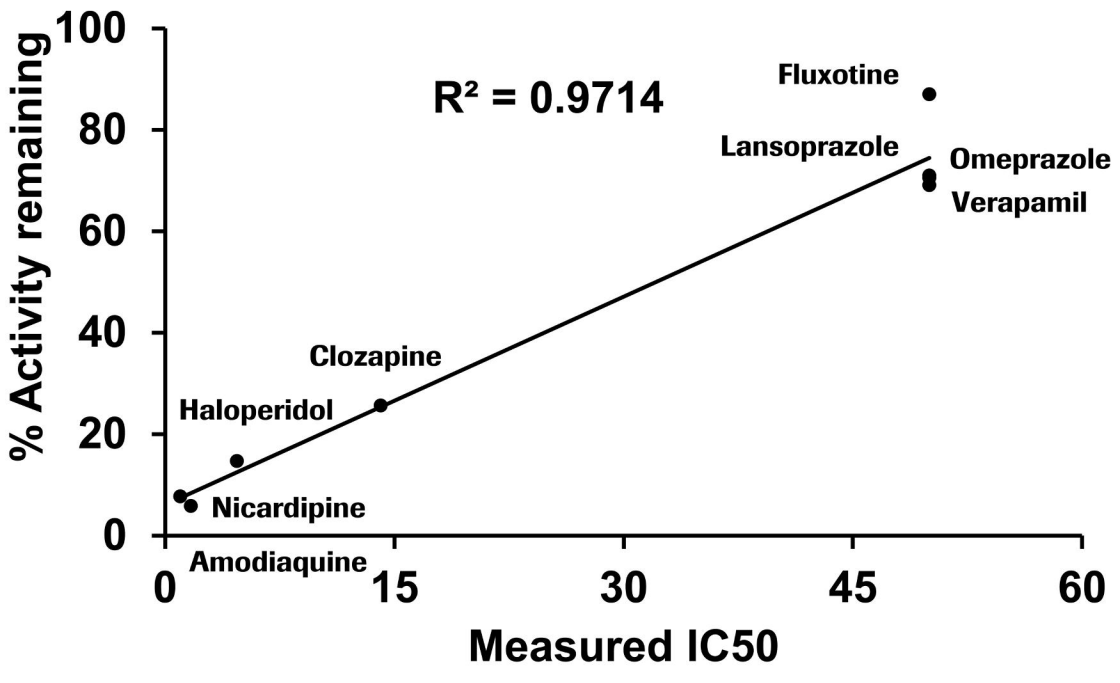
100
80
60
40
20
0
% Activity remaining
R² = 0.9714
Fluxotine
Lansoprazole
Omeprazole
Verapamil
Clozapine
Haloperidol
Nicardipine
Amodiaquine
0
15
30
45
60
Measured IC50

Figure 7

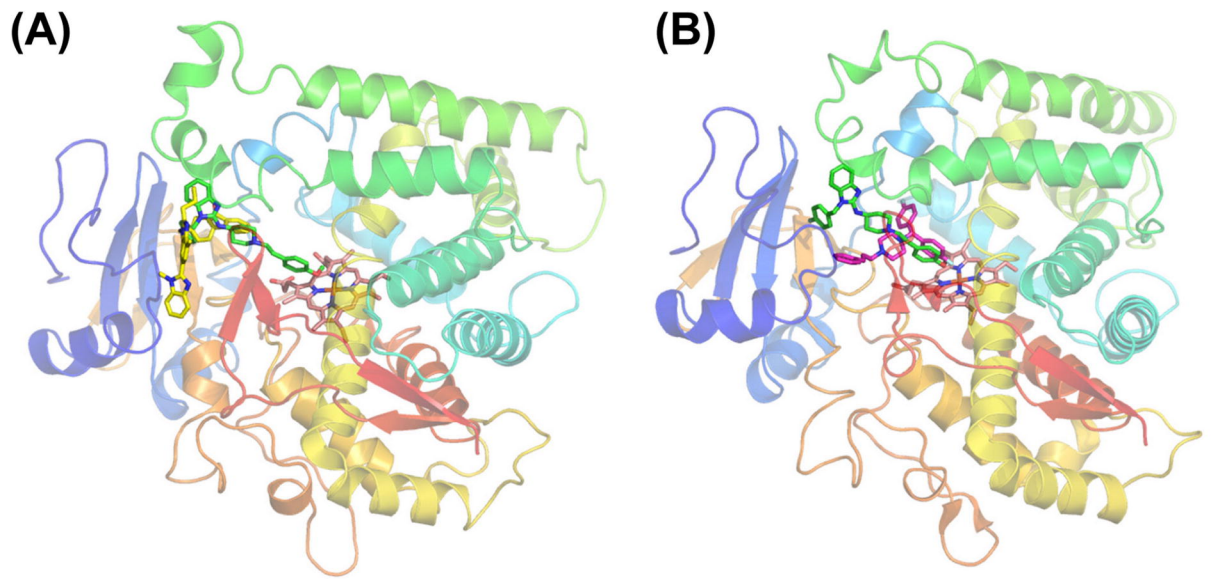

Figure 8